DESIGN AND IMPLEMENTATION OF VOLTAGE BASED HUMAN INSPIRED FEEDBACK CONTROL OF A PLANAR BIPEDAL ROBOT AMBER

A Thesis

by

MURALI KRISHNA PASUPULETI

Submitted to the Office of Graduate Studies of
Texas A&M University
in partial fulfillment of the requirements for the degree of

MASTER OF SCIENCE

August 2012

Major Subject: Electrical Engineering

DESIGN AND IMPLEMENTATION OF VOLTAGE BASED HUMAN INSPIRED FEEDBACK CONTROL OF A PLANAR BIPEDAL ROBOT AMBER

A Thesis

by

MURALI KRISHNA PASUPULETI

Submitted to the Office of Graduate Studies of
Texas A&M University
in partial fulfillment of the requirements for the degree of

MASTER OF SCIENCE

Approved by:

Chair of Committee,	Aaron D. Ames
Committee Members,	Aniruddha Datta
	John Valasek
	Prasad Enjeti
Head of Department,	Costas N. Georghiades

August 2012

Major Subject: Electrical Engineering

ABSTRACT

Design and Implementation of Voltage Based Human Inspired Feedback Control of A Planar Bipedal Robot AMBER. (August 2012)
Murali Krishna Pasupuleti, B.Tech, National Institute of Technology at Warangal
Chair of Advisory Committee: Dr. Aaron D. Ames

This thesis presents an approach towards experimental realization of underactuated bipedal robotic walking using human data. Human-inspired control theory serves as the foundation for this work. As the name, "human-inspired control," suggests, by using human walking data, certain outputs (termed human outputs) are found which can be represented by simple functions of time (termed canonical walking functions). Then, an optimization problem is used to determine the best fit of the canonical walking function to the human data, which guarantees a physically realizable walking for a specific bipedal robot. The main focus of this work is to construct a control scheme which takes the optimization results as input and delivers human-like walking on the real-world robotic platform - AMBER. To implement the human-inspired control techniques experimentally on a physical bipedal robot AMBER, a simple voltage based control law is presented which utilizes only the human outputs and canonical walking function with parameters obtained from the optimization. Since this controller does not require model inversion, it can be implemented efficiently in software. Moreover, applying this methodology to AMBER, experimentally results in robust and efficient "human-like" robotic walking.

DEDICATION

I dedicate this work to my family and friends who are very supportive of my education in USA and encouraged every effort of mine in the endeavor of completing my M.S. degree.

ACKNOWLEDGMENTS

I would like to thank Dr. Ames for his continuous support and advice that helped me throughout my M.S. program. I really appreciate his belief in my abilities and his valuable suggestions during our interactions which enabled me to understand the rigors of my research project. I also thank my dear friends Shishir, Mike, Jordan, and Ryan for being part of the AMBER team, without whom I cannot imagine this project to be successful. I also thank Eric, Huihua, Matt, Shu, Shawanee, Wenlong, Nathan, Ayonga for their valuable insights and support in various capacities and making my stay at AMBER lab an enjoyable experience. I also want to extend my sincere gratitude to my advisory committee — Dr. Datta, Dr. Enjeti and Dr. Valasek for their inputs in making this work a valuable contribution to the literature. I greatly appreciate Dr. Orsi of Oceanography Department who gave me an opportunity to work with him and his kind support during my first year at Texas A&M University. My thesis work is supported by NSF grants CNS-0953823 and CNS-1136104, and NHARP award 00512-0184-2009.

NOMENCLATURE

y_a	Actual outputs of the robot
(f_R, g_R)	Affine control system of hybrid system
θ	Angular configuration of the robot
$\dot{\theta}$	Angular velocity configuration of the robot
r_a	Armature resistance of DC motor
E_b	Back e.m.f of the DC motor
y_H	Canonical walking function
f_{cl}	Closed-loop control system
Q_R	Configuration space of the robot
(f_{Rv}, g_{Rv})	Control system with voltage input
ε	Controller gain
i_a	Current in the armature of DC motor
ω_d	Damped natural frequency
ζ	Damping ratio
A	Decoupling matrix
v_{hip}	Desired forward velocity of the hip
X_R	Domain of hybrid system
$(\theta^*, \dot{\theta}^*)$	Fixed point of the periodic orbit with control gain ε
HZD	Full hybrid zero dynamics surface
K_P	Gain matrix
h_R	Height of swing foot
y_α	Human-inspired output
$\mathscr{HC}_R$	Hybrid control system
J	Inertia of the rotor of DC motor
L_c	Length of calf link
L_t	Length of thigh link

L_{tor}	Length of torso link
B	Lie derivative
δp_{hip}	Linearized forward hip position
δp^R_{hip}	Linearized hip position of the robot
δm_{nsl}	Linearized non-stance leg slope
K_ω	Motor speed constant matrix
ω_n	Natural frequency
θ_{nsh}	Non-stance hip angle
θ_{nsk}	Non-stance knee angle
α^*	Optimization fit for canonical walking function w.r.t human data
α	Parameter vector
τ	Parameterized time
T	Period of the orbit
$\mathcal{O}$	Periodic orbit with fixed point
P	Poincaré map
$(\vartheta(\alpha), \dot{\vartheta}(\alpha))$	Point on the intersection of the HZD surface and the guard
Δ_R	Reset map of hybrid system
$\dot{\omega}$	Rotor angular acceleration of the DC motor
ω	Rotor angular speed of the DC motor
$2D$	Sagittal plane motion
U_R	Set of admissible controls
k_ω	Speed constant of the DC motor
θ_{sf}	Stance ankle angle
θ_{sh}	Stance hip angle
θ_{sk}	Stance knee angle
x	State space
S_R	Switching surface of hybrid system
TQ_R	Tangent space of the configuration space Q_R

K_φ	Torque constant matrix
k_φ	Torque constant of the DC motor
u	Torque input
θ_{tor}	Torso angle
B_v	Virtual friction
J_v	Virtual inertia
B	Viscous friction of DC motor
V_{in}	Voltage input
Z_α	Zero dynamics surface

TABLE OF CONTENTS

Page

Page

LIST OF TABLES

LIST OF FIGURES

FIGURE Page

FIGURE Page

1. INTRODUCTION

Humans intrinsically display the following five major characteristics during walking — efficiency, naturalism, stability, simplicity, and versatility. Humans are also exceptional at adapting their walking gait based on the nature of the terrain; this enables them to navigate locations that wheeled robots cannot go. Hence, to achieve bipedal robotic walking which can display various motion primitives, i.e., walking on flat-ground, slopes, stairs and uneven terrain, it is natural to look to human-data [1–4] for inspiration in the design of formal controllers. Though human walking is a result of complex neuro-muscular interactions, it seems that the aforementioned high-dimensional walking behavior can be characterized by low-dimensional representation; for example, human walking behavior on flat-ground and uneven terrain appears to be controlled by task-based central pattern generators in the spinal cord [5–8]. This special property motivates the construction of a human-inspired controller for bipedal robots, which can help robots to navigate like humans in the real-world environments. Thereby, this advancement paves the way for development of prosthetic legs which can help the lower limb amputees regain their normal walking gait. The philosophy behind this work is "simplicity implies robustness," so the main objective of this thesis is to develop a framework which can seamlessly integrate human walking data to design control algorithms which are simple, computationally tractable and therefore easily realizable on physical robots.

Numerous approaches which aim to find the underlying "simplicity" in bipedal walking have been explored. Some of the first fundamental work in this area was by Marc Raibert, with the idea of achieving locomotion through the use of inverted pendulum models to create single-legged hoppers [9], and Tad Mcgeer who introduced the concept of passive walking [10], which has also been realized on robots with efficient actuation [11]. Passive walking lead to the notion of controlled symmetries

---

This thesis follows the style of *IEEE Transactions on Control Systems Technology*.

[12], which allows for low energy walking, and the inverted pendulum models have led to the Spring Loaded Inverted Pendulum (SLIP) models for running robots [13–15]. In addition to these "minimalist" approaches, several methods have been proposed to directly bridge the gap between biomechanics and control theory by looking at human walking data to build models for bipedal robotic walking (see [16–18] to name a few). Finally, by combining many of the above approaches significant strides have been made in underactuated bipedal walking (no feet) by using the idea of virtual constraints and hybrid zero dynamics (HZD) [19, 20], which resulted in amazingly robust walking even on rough terrain.

Several experimental and commercial robotic models were built which aim to traverse flat-ground, uneven terrain, and sloped surfaces. Majority of them can be classified into the following groups: planar bipeds [20–22], humanoids [23–26], 3D bipeds [27–29] and bipeds with compliance [11, 30, 31]. While some of the planar bipeds mentioned do not have knees, other models including the 3D bipeds and humanoids use quasi-dynamic approaches leading them to very slow walking speed and marginal ability to reject disturbances. Only the robots with in-built compliance have displayed the power efficient and dynamically stable properties required for the robots to navigate environments where humans can go. However, adding compliance via the use of stiffness actuators (or) springs, increases the cost of the robot and complexity of control. Moreover, the robot structures are not extensible for building prosthetics. HZD based walking has shown promise in achieving fast response to large disturbances [30], and it represents bipedal walking in a very simple and elegant fashion. Implementing a HZD controller on a biped involves the determination of the parameters of the robot through identification experiments [32], which are not only very exhaustive and time consuming but are also not scalable to changes in hardware (or) robot structure.

This work attempts to overcome the limitations posed by a HZD controller (which uses traditional polynomial representations), by using outputs and canonical walk-

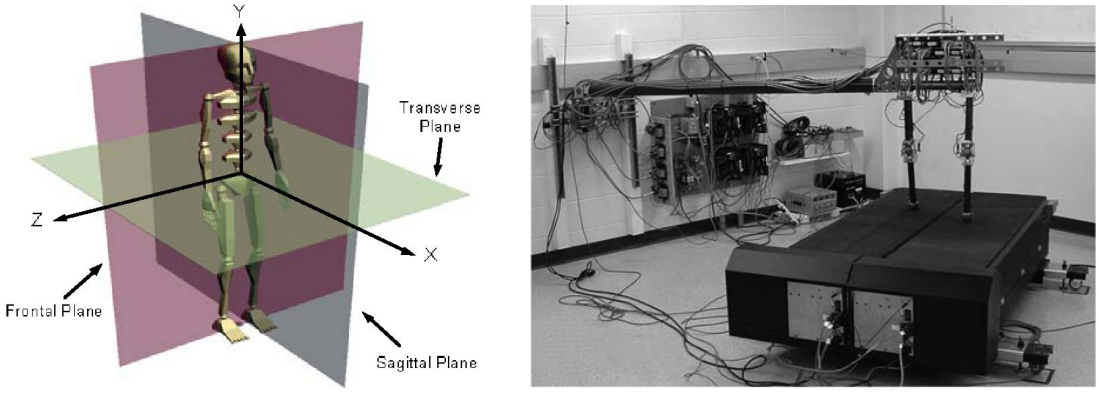

(a) (b)

Fig. 1.1.: (a.) Planes of motion for human body [33]. (b.) ERNIE [34].

ing functions which intrinsically capture the major characteristics of human walking behavior. The main contribution of this thesis is to design an experimental test bed - AMBER, which can serve as the foundation for the implementation of human-inspired control theory developed by Ames et. al [35, 36]. Human-inspired control approach on AMBER thus aims to further bridge the gap between robotics and control by using human walking data to formally design controllers (as first discussed in [35]). Specifically, by considering human walking data obtained through motion capture of subjects walking on flat ground, it was found that certain outputs (or virtual constraints) of the human as calculated from this data can be represented by a special class of functions, termed canonical walking functions and can be characterized as time response of a linear spring-mass-damper system. Thus, humans appear to act like linear spring-mass-damper systems when walking on flat-ground. By forming an optimization algorithm, where the cost is the least squares fit of the human walking functions to the human walking data, parameters for a human-inspired controller that provably results in stable underactuated robotic walking that is as close as possible to human walking are found. Utilization of similar off-line model-based optimization techniques to generate stable walking gaits have been explored in the past, for example see [19, 37, 38]. Using the human-inspired outputs which resulted

in stable robotic walking in simulation, on AMBER — an underactuated bipedal robot designed to walk in sagittal plane (Fig. 1.1a) — a simple voltage-based proportional (P) feedback control law on the outputs is defined. Since the actuators of AMBER are powered by DC motors, this naturally lends itself to simple implementation on the physical robot. The end result is that the voltage applied to the motors is directly proportional to the difference between the outputs of the robot and the outputs of the robot, as represented by the canonical walking functions. The experimental setup for this thesis is inspired from the earlier work on the following planar biped platforms: ERNIE and RABBIT (see Fig. 1.1b and 1.2a).

The goal behind experimentally implementing the formal results of the human-inspired control approach to bipedal robotic walking is to establish our hypothesis, that the inherent robustness present in the human outputs which are chosen, can be utilized to create simple and efficient feedback control strategies to enhance the design process for prosthetic legs. Experimental implementation of the algorithms developed on AMBER resulted in bipedal robotic walking that is efficient, robust and "human-like." Formal proof of the stability of the controller is out of scope of this work, but the stability of the proposed voltage-based control scheme is verified numerically through simulation studies by adding motor model to the hybrid model of the robot (see [39]). Voltage-based controllers with provable stability using adaptive control laws were explored for robotic manipulators [40, 41], but voltage-based approaches with formal stability proof for hybrid control systems are still an open problem. Using the proposed P-control, a very good agreement between the simulation and experimental data is observed, which indicates a direct connection between the formal methods and implementation. The experimental output data of the robot can also be related back to the human output data from which the controller was derived and for which there is a strong similarity showing that "human-like" walking is achieved. In addition to the stable walking, the robot exhibits robustness in walking even under the influence of a wide variety of disturbances like push-pull, knee strike,

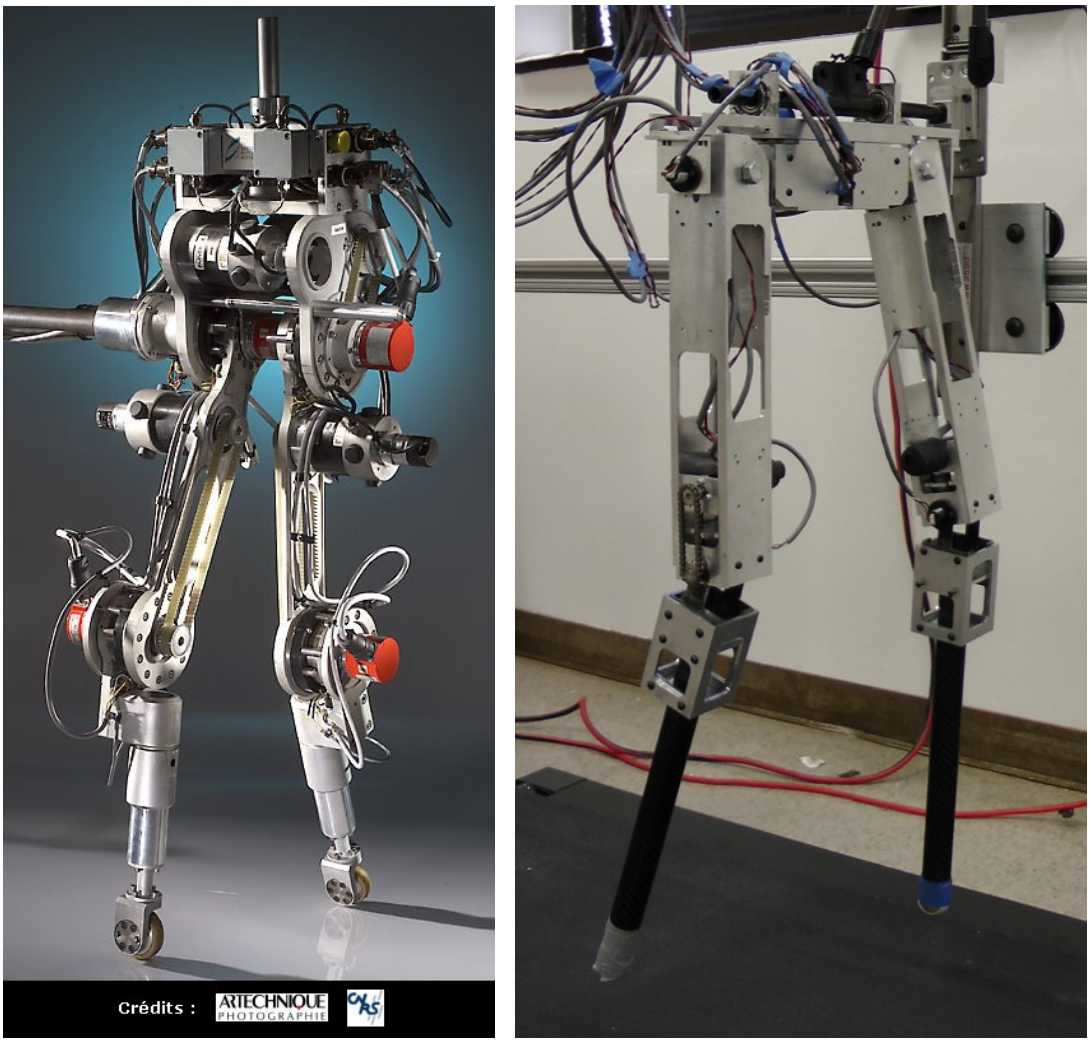

(a) (b)

Fig. 1.2.: (a.) RABBIT [19]. (b.) AMBER.

tripping, obstacles (as high as 6cm) and even with hits from wooden blocks (see [42]). This complex feat of robust walking was achieved by using minimal actuation and simple sensors — low power DC motors (11 W), position encoders and contact switches. Hence, simplicity of the voltage-based P-control on human-inspired outputs adheres closely to the philosophy that "simplicity implies robustness," this renders the walking algorithm and the resulting robotic walking efficient and robust.

The remainder of this thesis is organized into four chapters. Chapter 2 will present the mathematical modeling for the AMBER (see Fig. 1.2b), i.e., description of domains, guards, constraints and reset maps for a 5-link planar robot. Once the hybrid control system model of AMBER is represented, an overview of the human-inspired control for AMBER is presented. Chapter 3 presents the walking obtained in simulation using human-inspired optimization with constraints and describes the methodology behind selection of voltage-based approach with identification experiments on AMBER. In Chapter 4, the voltage-based proportional control law on canonical walking functions is presented along with the flowcharts of algorithms used for experimental implementation. After having achieved walking using P-control, a comparison is made between the walking obtained in the simulation and the one obtained in the physical biped. This is followed by conclusions with scope for future work in Chapter 5.

2. HUMAN-INSPIRED CONTROL FOR AMBER

AMBER (short for **A** & **M** **B**ipedal **E**xperimental **R**obot) is a 2D bipedal robot with 5 links (2 calves, 2 thighs and a torso, see Fig. 2.1). AMBER is 61cm tall with a total mass of 3.3Kg. It is made from aluminum with carbon fiber calves, powered by 4 Maxon DC motors and controlled through LabVIEW^{TM} software by National Instruments. The robot has point feet, and is thus underactuated at the ankle. In addition, since this robot is built for only 2D walking, it is supported in the lateral plane via a boom; this boom does *not* provide support to the robot in the sagittal plane. This means that the torso, through which the boom supports the robot, can freely rotate around the boom. The boom is fixed rigidly to a sliding mechanism (see Fig. 2.1), which allows the boom and consequently the biped, to move its hip front, back, up and down with minimum friction. The sliding mechanism is rested on a pair of parallel rails.

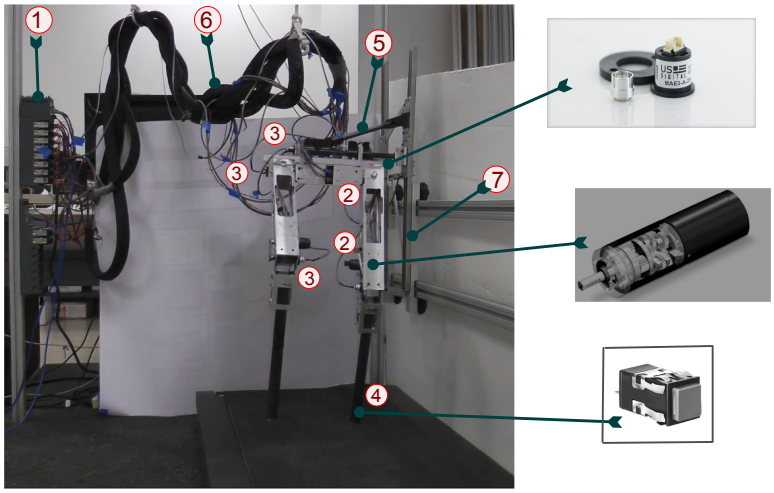

Fig. 2.1.: AMBER experimental setup. Parts marked are (1): NI cRIO, (2): Maxon DC motors located in the calf and the torso, (3): Encoders on boom and the joints, (4): Contact switch at the end of the foot, (5): Boom, (6): Wiring with sheath protection, (7): Slider for restricting the motion to the sagittal plane.

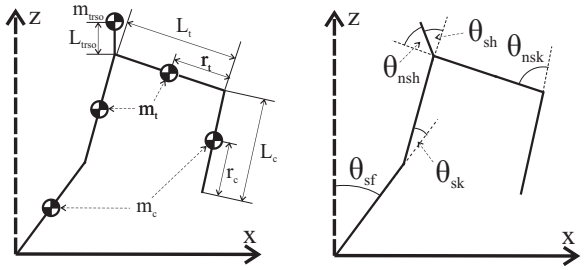

(a) (b)

Model Parameters				
Parameter	Mass g	Length mm	Inertia x-axis $\times 10^3\ g\ mm^2$	Inertia z-axis $\times 10^3\ g\ mm^2$
Stance calf	213.79	312.27	1967.37	119.69
Stance knee	606.15	282.37	6494.94	418.37
Torso	804.83	9.97	3730.23	3577.19
Non-stance knee	606.15	282.37	6494.94	418.37
Non-stance calf	213.79	312.37	1967.37	119.69

(c)

Fig. 2.2.: Notations used for (a.) masses and lengths of the links and (b.) angle conventions. (c.) Table with the masses, lengths and inertia properties for AMBER.

Let L_c, L_t, L_{tor} be the lengths of the calf, thigh and torso respectively (as shown in Fig. 2.2a) and $\theta = (\theta_{sf}, \theta_{sk}, \theta_{sh}, \theta_{nsh}, \theta_{nsk})^T$ be the angles of stance foot (foot of the stance leg), stance knee (knee of the stance leg), stance hip, non-stance (swing leg) hip and non-stance knee respectively. These variables form the configuration space of the robot, Q_R, and are shown in Fig. 2.2b. The parameter values which are used for modeling purposes are presented in Fig. 2.2c. Note that every time the swing foot hits the ground, the stance and non-stance nomenclatures are switched in the physical biped.

2.1 Hybrid Systems

Formally, the bipedal robot can be represented as a hybrid system (see [35,36,43] for a formal definition):

$$\mathscr{HC}_R = (X_R, U_R, S_R, \Delta_R, f_R, g_R), \tag{2.1}$$

where $X_R \subset TQ_R$ is the domain given by the constraint $h_R \geq 0$, where h_R is the height of the swing foot, $U_R \subset \mathbb{R}^4$ is the set of admissible controls, $S_R \subset X_R$ is the guard given by $h_R = 0$, Δ_R is the reset map which provides an instantaneous change in velocity at foot strike, and $\dot{x} = f_R(x) + g_R(x)u$, with $x = (\theta^T, \dot{\theta}^T)^T \in \mathbb{R}^{10}$ and u the torque input, is a control system obtained from the Lagrangian of the robot (which includes the mass and inertia of all links, the motors and the boom). Since the robot is controlled by DC motors, the controller design takes into consideration of the DC motor models which results in the control system $\dot{x} = f_{R_v}(x) + g_{R_v}(x)V_{in}$ with voltage, V_{in}, being the control input (see [44] for more information on modeling of AMBER).

2.2 Periodic Orbits

By applying the input (u or V_{in}) derived from the feedback controller, if it leads to bipedal robotic walking then it corresponds to stable periodic orbits in hybrid systems. For simplicity, only periodic orbits of hybrid systems with fixed points on the guard (for more general definitions, see [43, 45]) is presented. Let $\varphi(t, x_0)$ be the solution to $\dot{x} = f_{cl}(x)$ with initial condition $x_0 \in X_R$, where $f_{cl}(x)$ is the closed-loop control system representation. For $x^* \in S_R$, φ is *periodic* with period $T > 0$ if $\varphi(T, \Delta(x^*)) = x^*$. A set $\mathcal{O}$ is a *periodic orbit* with *fixed point* x^* if $\mathcal{O} = \{\varphi(t, x^*) : 0 \leq t \leq T\}$ for a periodic solution φ. Associated with a periodic orbit is a

Poincaré map [45]. In particular, taking S_R to be the Poincaré section, one obtains the Poincaré map $P : S_R \to S_R$ which is a partial function:

$$P(x) = \varphi(T_I(x), \Delta(x)),$$

where T_I is the *time-to-impact function* [19]. As with smooth dynamical systems, the stability of the Poincaré map determines the stability of the periodic orbit $\mathcal{O}$. In particular, the Poincaré map is (locally) exponentially stable (as a discrete time system $x_{k+1} = P(x_k)$) at the fixed point x^* if and only if the periodic orbit $\mathcal{O}$ is (locally) exponentially stable [46]. Although it is not possible to analytically compute the Poincaré map, it is possible to numerically compute its Jacobian. Thus, if the eigenvalues of the Jacobian have magnitude less than one, the stability of the periodic orbit $\mathcal{O}$ has been numerically verified.

2.3 Human Walking Experiment

The data presented in this thesis was collected using the Phase Space System. It consisted of 12 high precision cameras positioned to allow 3D spatial measurements of a number of LED sensors to an accuracy within one millimeter. The positions of the sensors were collected at 480 Hz. Prior to the experiment the cameras were calibrated and placed to achieve a millimeter level of accuracy for a space of 5 by 5 by 5 meters cubed. 8 LED sensors were placed on each leg as pictured in Fig. 2.3, with 1 LED sensor placed on the front and back sternum as well as the navel. Each trial of the experiment required the subject to walk 3 meters along a line drawn on the floor. Each subject performed 11 trials in a single experiment. Overall, data was collected from 9 subjects: 2 female and 7 male subjects with ages ranging between 17 and 30, heights ranging between 160.0cm and 188.5cm, and weights ranging between 47.7kg and 90.9kg. Note that the human data is collected from two experiments separately. The data of the first 5 subjects is taken from one experiment and the

Fig. 2.3.: Straight line human walking experiment with LED sensors placed on various sections of the human subject.

data for the other 4 subjects is collected from the experiment one year later. The two experiments have the same setup and took place at the same lab. Although the data is collected from two experiments, the analysis results are the same. This fact shows that the data analysis processing algorithm is repeatable. The walking tile for the post-processed mean human walking data, which is used to design human-inspired controllers is presented in Fig. 2.4.

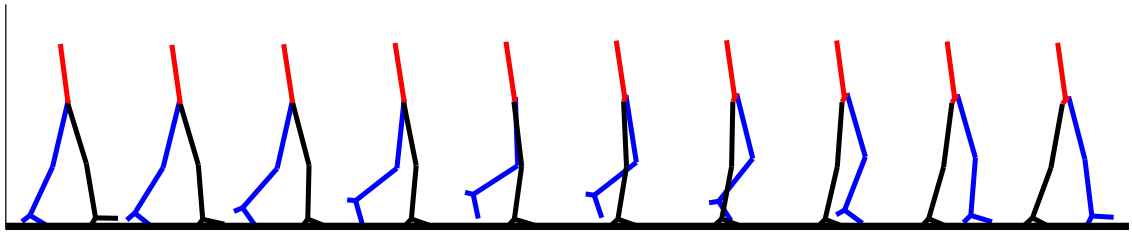

Fig. 2.4.: Walking tile using mean human data obtained from the human walking experiments.

2.4 Human-Inspired Functions

By considering human walking data (as described in [35]), its found that certain outputs (or virtual constraints), computed from the human joint data, display simple behavior; this core observation will be central to the design of human-inspired controllers. The goal of picking the outputs is to elucidate the underlying structure of walking through a low-dimensional representation. In particular, the following collection of outputs yields such a representation:

1. The linearization of the x-position of the hip, p_{hip}, given by:

$$\delta p_{\text{hip}}(\theta) = L_c(-\theta_{sf}) + L_t(-\theta_{sf} - \theta_{sk}), \tag{2.2}$$

2. The linearization of the slope of the non-stance leg m_{nsl}, (the tangent of the angle between the z-axis and the line on the non-stance leg connecting the ankle and hip), given by:

$$\delta m_{nsl}(\theta) = -\theta_{sf} - \theta_{sk} - \theta_{sh} + \theta_{nsh} + \frac{L_c}{L_c + L_t}\theta_{nsk}. \tag{2.3}$$

3. The angle of the stance knee, θ_{sk},

4. The angle of the non-stance knee, θ_{nsk},

5. As mentioned above, the angle of the torso from vertical,

$$\theta_{tor}(\theta) = \theta_{sf} + \theta_{sk} + \theta_{sh}. \tag{2.4}$$

It is important to note that the linearized form of these outputs, rather than their original nonlinear form [35], is considered to allow for more efficient software implementation.

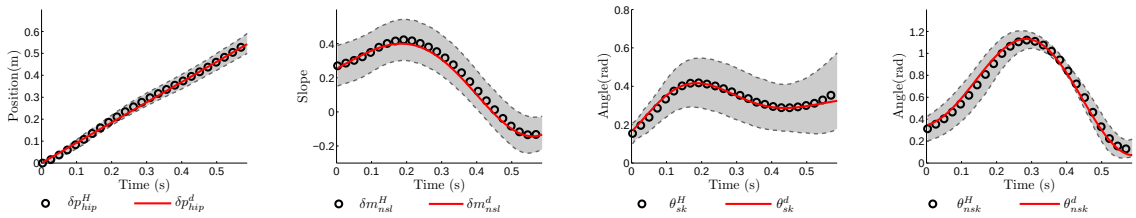

(a) Linear hip position (b) Non-stance slope (c) Stance Knee (d) Non-stance Knee

Fig. 2.5.: Mean of the trajectories of the human outputs from all test subjects put together. The grey shaded area indicates the standard deviation from the mean trajectory. The red lines are the fits of the canonical walking functions to the mean human data.

Inspection of these outputs, as computed from the human data and shown in Fig. 2.5, reveals that they appear to display very simple behavior. In the case of the (linearized) position of the hip, it appears to essentially be a linear function of time:

$$\delta p^d_{\text{hip}}(t, v) = v_{hip} t, \tag{2.5}$$

The remaining outputs, (the non-stance slope δm_{nsl}, the stance knee θ_{sk}, the non-stance knee θ_{nsk} and the torso angle θ_{tor}) appear to act like a second order linear system. This motivated the introduction of the *canonical walking function* [36]:

$$y_H(t, \alpha) = e^{-\alpha_4 t}(\alpha_1 \cos(\alpha_2 t) + \alpha_3 \sin(\alpha_2 t)) + \alpha_5. \tag{2.6}$$

which is simply the time solution to a linear mass-spring damper system, with $\alpha_4 = \zeta\omega_n$, where ζ is the damping ratio and ω_n is the natural frequency, $\alpha_2 = \omega_d$, where $\omega_d = \omega_n\sqrt{1-\zeta^2}$ is the damped natural frequency, $\alpha_1 = c_0$ and $\alpha_3 = c_1$, where c_0, c_1 are determined by the initial conditions of the system and $\alpha_5 = g$, where g is the gravity related constant. Performing a least squares fit of the human output data with these functions results in near unity correlations, implying that for the specific outputs chosen humans appear to act like linear mass-spring-damper systems.

This is an important conclusion because it illustrates the simplicity in behavior that humans display when walking. Moreover, utilizing these functions in the control implementation on AMBER will result in behavior that mimics "compliant systems" even without the mechanical use of springs and dampers.

2.4.1 Human-Inspired Outputs

Having obtained outputs from the inspection of human data, the goal will be to construct a controller that drives the outputs of the robot to the outputs of the human, as represented by the canonical walking function: $y_a(\theta(t)) \to y_d(t, \alpha)$, with:

$$y_d(t,\alpha) = \begin{bmatrix} y_H(t,\alpha_{nsl}) \\ y_H(t,\alpha_{sk}) \\ y_H(t,\alpha_{nsk}) \\ y_H(t,\alpha_{tor}) \end{bmatrix}, \qquad y_a(\theta) = \begin{bmatrix} \delta m_{nsl}(\theta) \\ \theta_{sk} \\ \theta_{nsk} \\ \theta_{tor}(\theta) \end{bmatrix}, \tag{2.7}$$

where $y_H(t, \alpha_i)$, $i \in \{nsl, sk, nsk, tor\}$ is the canonical walking function (2.6) but with parameters, α_i specific to the output being considered. By grouping these parameters with the velocity of the hip, v_{hip}, that appears in (2.5) results in the vector of parameters $\alpha = (v_{hip}, \alpha_{nsl}, \alpha_{sk}, \alpha_{nsk}, \alpha_{tor})$.

In order to remove the time dependence of $y_d(t, \alpha)$, the time is parameterized using the (linearized) position of the hip as it's accurately described by a linear function of time. This motivates the following parametrization of time:

$$\tau(\theta) = \frac{\delta p^R_{\text{hip}}(\theta) - \delta p^R_{\text{hip}}(\theta^+)}{v_{\text{hip}}}, \tag{2.8}$$

where $p^R_{\text{hip}}(\theta^+)$ is the position of the hip of the robot at the beginning of a step[1] where θ^+ is a point where the height of the non-stance foot is zero, i.e., $h_R(\theta^+) = 0$. Using the parametrization of time, the *human-inspired output* is defined as follows:

$$y_\alpha(\theta) = y_a(\theta) - y_d(\tau(\theta), \alpha), \tag{2.9}$$

2.4.2 Human-Inspired Control

Consider again the affine control system (f_R, g_R) associated with the hybrid model of AMBER (2.1). The human outputs were explicitly chosen so that the decoupling matrix, $A(\theta, \dot\theta) = L_{g_R} L_{f_R} y_\alpha(\theta, \dot\theta)$ with L the Lie derivative, is nonsingular. Therefore, the human-inspired outputs are (vector) relative degree 2, hence a torque-based controller can be defined as:

$$u_{(\alpha,\varepsilon)}(\theta, \dot\theta) = -A^{-1}(\theta, \dot\theta) \left(L^2_{f_R} y_\alpha(\theta, \dot\theta) + 2\varepsilon L_{f_R} y_\alpha(\theta, \dot\theta) + \varepsilon^2 y_\alpha(\theta) \right). \tag{2.10}$$

In other words, input/output linearization (see [47]) is applied to obtain the linear system on the human-inspired outputs: $\ddot y_\alpha = -2\varepsilon \dot y_\alpha - \varepsilon^2 y_\alpha$. This system is exponentially stable, implying that for $\varepsilon > 0$ the control law $u_{(\alpha,\varepsilon)}$ drives $y_\alpha \to 0$. More generally, it renders the *zero dynamics surface*:

$$\mathbf{Z}_\alpha = \{(\theta, \dot\theta) \in TQ_R : y_\alpha(\theta) = \mathbf{0},\ \ L_{f_R} y_\alpha(\theta, \dot\theta) = \mathbf{0}\} \tag{2.11}$$

invariant and exponentially stable for the *continuous dynamics*. Yet this property does not hold for the hybrid dynamics since discrete impacts in the system cause the state to be "thrown" off of the zero dynamics surface. Therefore, the goal is to achieve *hybrid zero dynamics*: $\Delta_R(S_R \cap \mathbf{Z}_\alpha) \subset \mathbf{Z}_\alpha$, i.e., render the zero dynamics

[1]Note that we can assume that the initial position of the human is zero, while this cannot be assumed for the robot since the initial position of the hip will depend on the specific choice of configuration variables for the robot.

surface invariant through impact. This will imply that the behavior of the robot will be characterizable by the "virtual model" that motivated the output functions under consideration, and will thus allow us to guarantee the existence of walking gaits.

2.4.3 Optimization Algorithm

This section presents the main theorem that will be used to generate the control parameters that will be experimentally implemented on AMBER to obtain robotic walking. From the mean human walking data, discrete times, $t^H[k]$, and discrete values for the human output data, $y_i^H[k]$ and the canonical walking functions, $y_i^d(t, \alpha_i)$ for $i \in \text{Output} = \{hip, nsl, sk, nsk, tor\}$ are obtained; for example, $y_{nsl}^H[k] = y_H(kT, \alpha_{nsl})$, where T is the discrete time interval and $k \in \mathbb{Z}$. Then the following human-data cost function is defined:

$$\text{Cost}_{\text{HD}}(\alpha) = \sum_{k=1}^{K} \sum_{i \in \text{Output}} \left(y_i^H[k] - y_i^d(t^H[k], \alpha_i) \right)^2 \tag{2.12}$$

which is simply the sum of squared residuals. To determine the parameters for the human walking functions, the following optimization problem is solved:

$$\alpha^* = \underset{\alpha \in \mathbb{R}^{21}}{\text{argmin}} \ \text{Cost}_{\text{HD}}(\alpha) \tag{2.13}$$

which yields the least squares fit of the mean human output data with the canonical walking functions. While this provides a α^* that yields a good fit of the human data (see Fig. 2.5), these parameters will not result in robotic walking due to the differences between the robot and a human. Therefore, the goal is to determine these parameters which provide the best fit of the human data while simultaneously guaranteeing stable robotic walking for AMBER. This motivates the following theorem:

Theorem 2.4.1 *The parameters α^* solving the constrained optimization problem [35, 36]:*

$$\alpha^* = \underset{\alpha \in \mathbb{R}^{21}}{\operatorname{argmin}} \ \operatorname{Cost}_{\mathrm{HD}}(\alpha) \tag{2.14}$$

$$\text{s.t} \quad y(\vartheta(\alpha)) = \mathbf{0} \tag{C1}$$

$$dy_\alpha(\Delta_\theta \vartheta(\alpha))\Delta_{\dot\theta}(\vartheta(\alpha))\dot\vartheta(\alpha) = \mathbf{0} \tag{C2}$$

$$dh_R(\vartheta(\alpha))\dot\vartheta(\alpha) < 0 \tag{C3}$$

$$\mathcal{D}_{\mathbf{Z}}(\vartheta(\alpha)) < 0 \tag{C4}$$

$$0 < \Delta_{\mathbf{Z}}(\vartheta(\alpha)) < 1 \tag{C5}$$

yield hybrid zero dynamics: $\Delta_R(S_R \cap \mathbf{Z}_{\alpha^*}) \subset \mathbf{Z}_{\alpha^*}$. Moreover, there exists an $\hat\varepsilon > 0$ such that for all $\varepsilon > \hat\varepsilon$ the hybrid system $\mathscr{H}_R^{(\alpha^*,\varepsilon)}$, obtained by applying the control law (2.10) *to the hybrid control system* (2.1)*, has a stable periodic orbit with fixed point $(\theta^*, \dot\theta^*) \in S_R \cap \mathbf{Z}_{\alpha^*}$ that can be explicitly computed.*

A detailed explanation of all the elements utilized in this Theorem can be found in [36]. Of particular importance is the point $(\vartheta(\alpha), \dot\vartheta(\alpha)) \in S_R \cap \mathbf{Z}_\alpha$ which is a point on the intersection of the zero dynamics and the guard that can be explicitly computed in terms of the parameters α. This point is used to ensure hybrid zero dynamics through (C1)-(C3), and guarantees the existence of a stable periodic orbit in the zero dynamics surface through (C4) and (C5) which implies the existence of a stable walking gait for sufficiently large ε.

The walking gait of the robot that we achieve using Theorem 2.4.1 should also be physically realizable. In particular, constraints that demand torques (2 Nm) and angular velocities (6.5 rad/s) that are within the limits of the DC motors, produce a good step length, and most importantly prevent the swing foot from scuffing (which appears to directly relate to stability of the walking gait) are added to the optimization problem which ensures that the resulting control parameters will ex-

perimentally result in walking with AMBER. More details on formulation of the optimization problem with physical realizability conditions and results can be found in [35, 36, 39].

3. EVOLUTION OF CONTROL LAW IMPLEMENTATIONS FOR AMBER

There are numerous methods for achieving stable and sustainable robotic walking, starting from passive walking to using controlled symmetries to following a certain set of trajectories (see [48], [10], [19] and [11]). Since the objective of this thesis is to achieve walking in an underactuated robot (without feet), it is natural to look to the seminal work of Grizzle et. al which builds upon the concept of tracking parameterized trajectories described by Bézier polynomials [19]. But before doing that, Ames et. al decided to look at humans for getting inspiration for walking [49]. Even though it is hard, it is important to understand and make a detailed and a comprehensive analysis of human walking. That was how the concept of human-inspired control was born. Capturing and observing the data from human walking experiments was the next logical step and the coming sections will explain in detail about the evolution of the control laws used to experimentally achieve the goal of robust and stable "human-like" robotic walking on AMBER using human walking data.

By implementing the human-inspired optimization problem i.e., Theorem 2.4.1 in MATLAB$^{\text{TM}}$, the resulting optimized parameters α^* (see Table 3.1) yields a hybrid system which satisfies the HZD criterion and physical realizability conditions. Moreover, the same optimization automatically generates a fixed point to a stable periodic orbit; this is verified by picking $\varepsilon = 10$ in (2.10) and checking the eigenvalues of the linearization of the Poincaré map for which the maximum magnitude is 0.8286 (and hence less than 1). The periodic orbits, outputs and joint angles of the walking gait obtained are shown in Fig. 3.1a, 3.1b and 3.1c respectively. Fig. 3.1d shows that the torques are well within the limits, 2 Nm; which consequently means that the canonical walking functions are definitely realizable, to obtain robotic walking on AMBER.

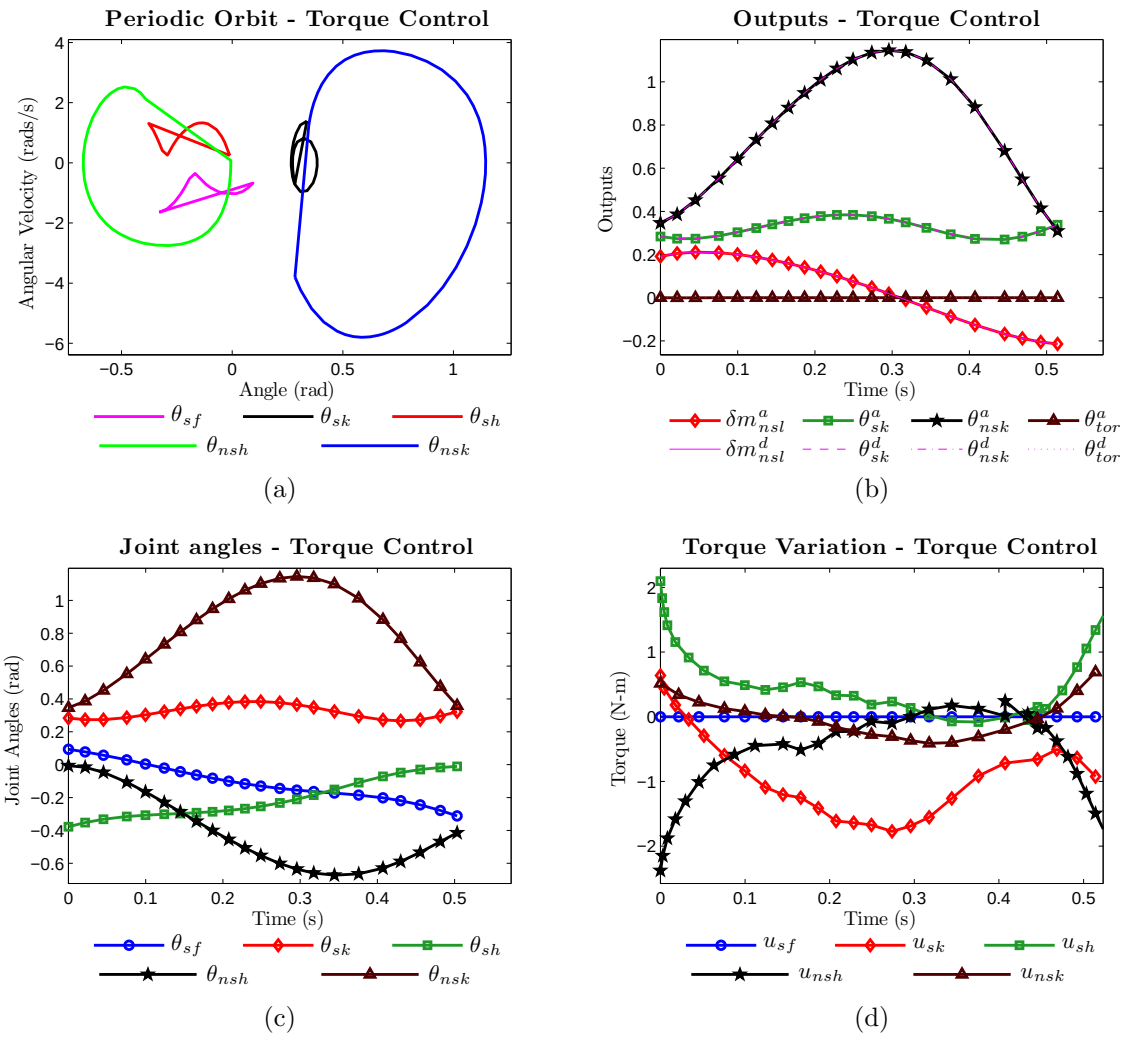

Fig. 3.1.: (a.) Phase portraits for the walking gait obtained from simulation using human-inspired control. (b.) Canonical walking functions resulting from the human-inspired optimization with constraints. (c.) Joint angles and (d.) torque input trajectories for a single step of the robot walking in simulation using input/output linearization technique [44].

3.1 Time-based Tracking Controller on Angles

Using the hip and knee angle trajectories (Fig. 3.1c) obtained from simulating robotic walking using torque-based human-inspired control, a PID controller (as shown in Fig. 3.2) is implemented in LabVIEW, to validate the physical realizability

Table 3.1: Table containing parameter values of the canonical human walking functions obtained from running the human-inspired optimization with the constraints [44].

$y_H = e^{-\alpha_4 t}(\alpha_1 \cos(\alpha_2 t) + \alpha_3 \sin(\alpha_2 t)) + \alpha_5$							
Fun.	v_{hip}	α_1	α_2	α_3	α_4	α_5	Cor.
δp_{hip}	0.4401	*	*	*	*	*	0.9991
δm_{nsl}	*	0.2374	6.0244	0.1346	0.7820	-0.0459	0.8899
θ_{sk}	*	-0.0436	15.6312	-0.0320	-0.2430	0.3271	0.8180
θ_{nsk}	*	-0.3632	-9.6707	-0.1165	-0.4538	0.7097	0.9891
θ_{tor}	*	-0.0000	-0.0000	0	0	-0.0000	0

of the human-inspired control theory. As the controller implements a time-based tracking technique, it has no disturbance rejection in state space i.e., it has no guarantee of achieving sustained and stable periodic walking behavior. Owing to the strength of human-inspired optimization technique to produce a walking gait which satisfies the torque and angular velocity constraints, trajectory tracking consistently resulted in 5-10 steps of robotic walking on AMBER. Fig. 3.3 shows the walking tile of AMBER for a single step with this controller. This initial step towards successfully implementing the results of human-inspired control theory experimentally, served as an impetus to explore for a more robust state-based feedback control solution.

3.2 System Identification Experiments for Voltage-based Control

For obtaining dynamically stable bipedal walking, torque-based PD control on output functions (or virtual constraints) is widely used (see [50]). With electric motors, implementing a torque-based controllers involves a secondary control loop which generates a voltage equivalent to the current (torque) set-point generated from the primary PD control. Moreover, for bipeds with electrical actuators, the hybrid control system models doesn't take into account of the motor parameters, which can lead to higher control costs. Torque-based approach has two stages of control to produce a voltage input, which requires additional hardware resources and

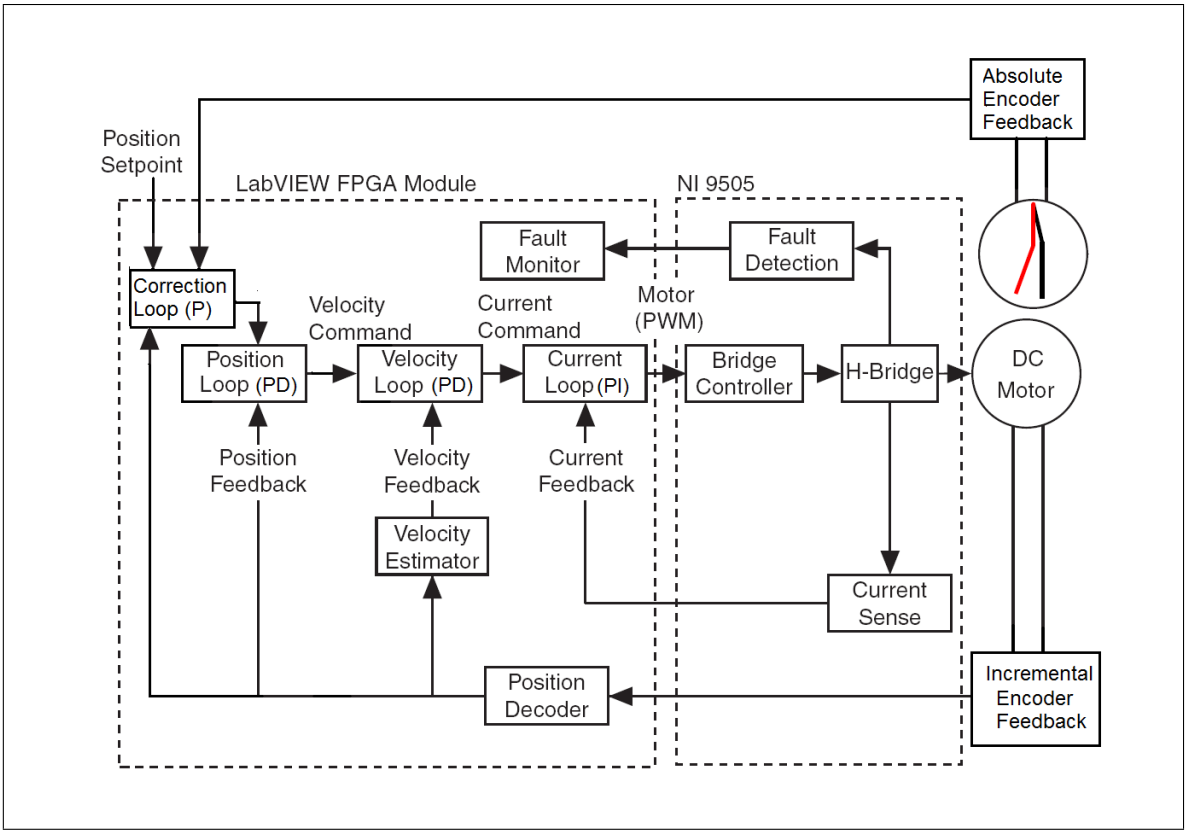

Fig. 3.2.: PID tracking controller on angle trajectories (see Fig. 3.1c), derived from the simulation of AMBER walking.

sensors. Hence, an alternative approach which can directly produce the voltage to the electric motor with minimal sensing is considered. This section presents the system identification experiments on AMBER, conducted for the purpose of validating a direct voltage-based DC motor control approach to obtain robotic walking. The experimental identification data in conjunction with the desired dynamic walking gait properties of AMBER — speed and acceleration data (obtained from simulated walking shown in Fig. 3.1), gives directly the voltage input. Voltage equivalent of the desired torque for the same walking gait (Fig. 3.1), is considered to highlight the effectiveness of the proposed direct voltage-based approach.

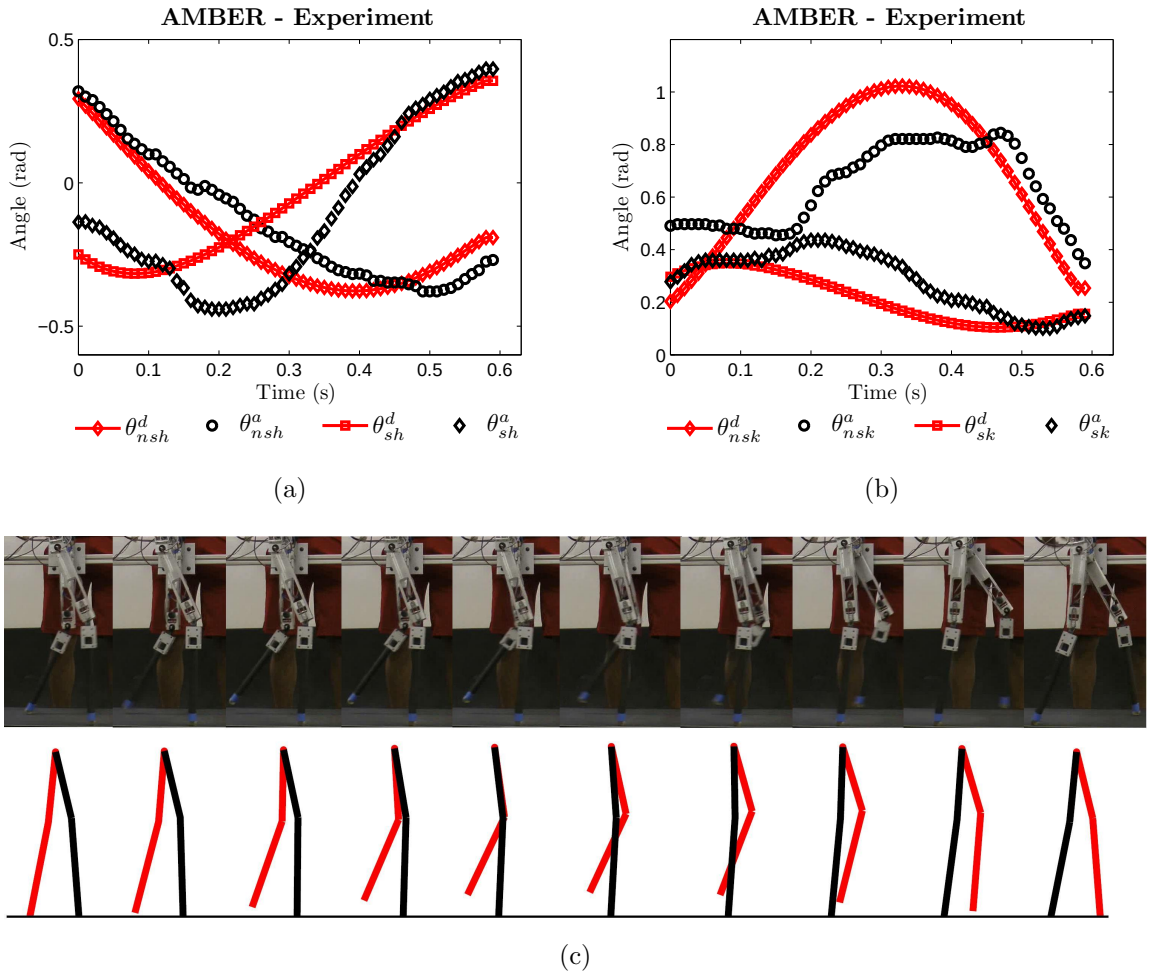

Fig. 3.3.: Trajectory tracking results for AMBER, experiment vs simulation: (a.) hip angles, (b.) knee angles and (c.) walking tile over one step.

For DC motors with small inductance, the voltage (V_{in}) required is given by:

$$V_{in} = i_a r_a + E_b \tag{V1}$$

$$E_b = k_\omega \omega \tag{V2}$$

$$k_\varphi i_a = J\dot{\omega} + B\omega \tag{V3}$$

where i_a is current in the motor armature, r_a is armature resistance, E_b is back e.m.f, k_ω is speed constant, k_φ is torque constant, ω is speed, J is inertia and B is friction

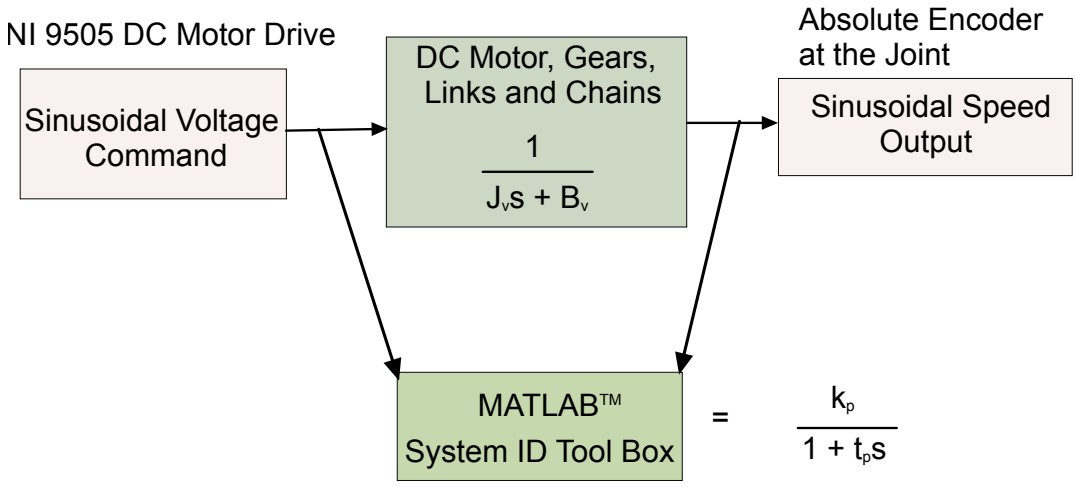

Fig. 3.4.: Block diagram of the identification experiment carried out for a configuration under test.

coefficient of motor and load. Substituting the value of i_a from V3 into V1, we have V4, whose transfer function is given by V5.

$$V_{in} = J_v\dot{\omega} + B_v\omega \tag{V4}$$

$$V_{in}(s) = \frac{k_p\omega(s)}{1 + t_p s} \tag{V5}$$

where J_v is virtual inertia and B_v is virtual friction of load, gearbox and motor reflected towards the motor end, $k_p = \frac{1}{B_v}$ and $t_p = \frac{J_v}{B_v}$. The form of V5 (first-order transfer function), is amenable for the system identification procedures as shown in Fig. 3.4.

Configuration of various combinations for the identification experiments carried out is given in Fig. 3.5. Feeding a reference sinusoidal voltage input to the motor and recording the speed at the motor end (see Fig. 3.6), the parameters k_p, t_p can be found for all the links actuated by the motors. The data recorded in every experiment is given to System Identification Toolbox in MATLAB^{TM} [51], which gives the coefficients— k_p, t_p of the linear model between voltage and angular velocity

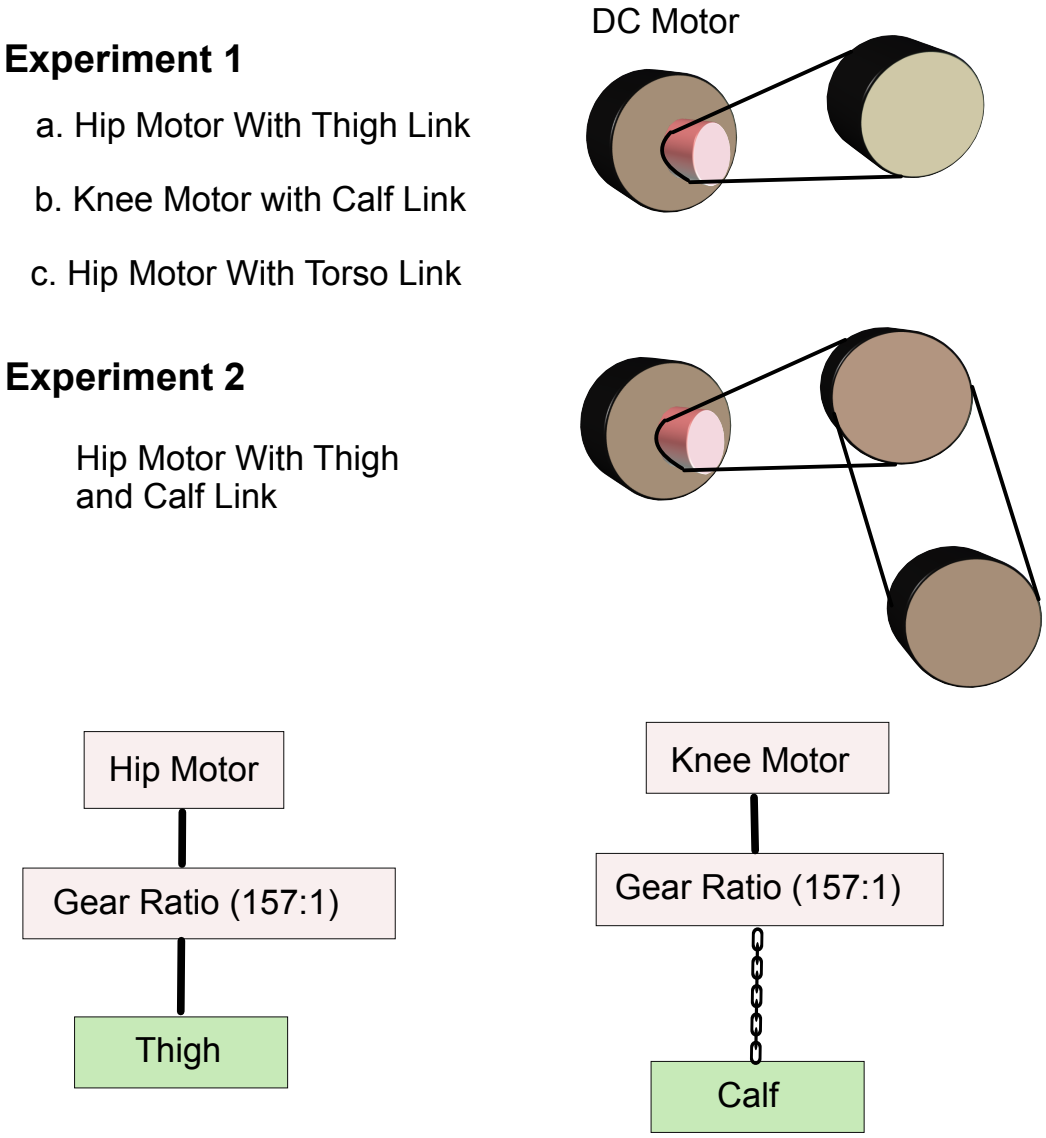

Fig. 3.5.: Configurations for the various identification experiments carried out on AMBER. Transmission mechanism used for knee links is chain and sprocket, while hips are directly driven by the DC motor.

from which values for J_v and B_v are calculated. The identified data collected for all the joints is tabulated in Table 3.2.

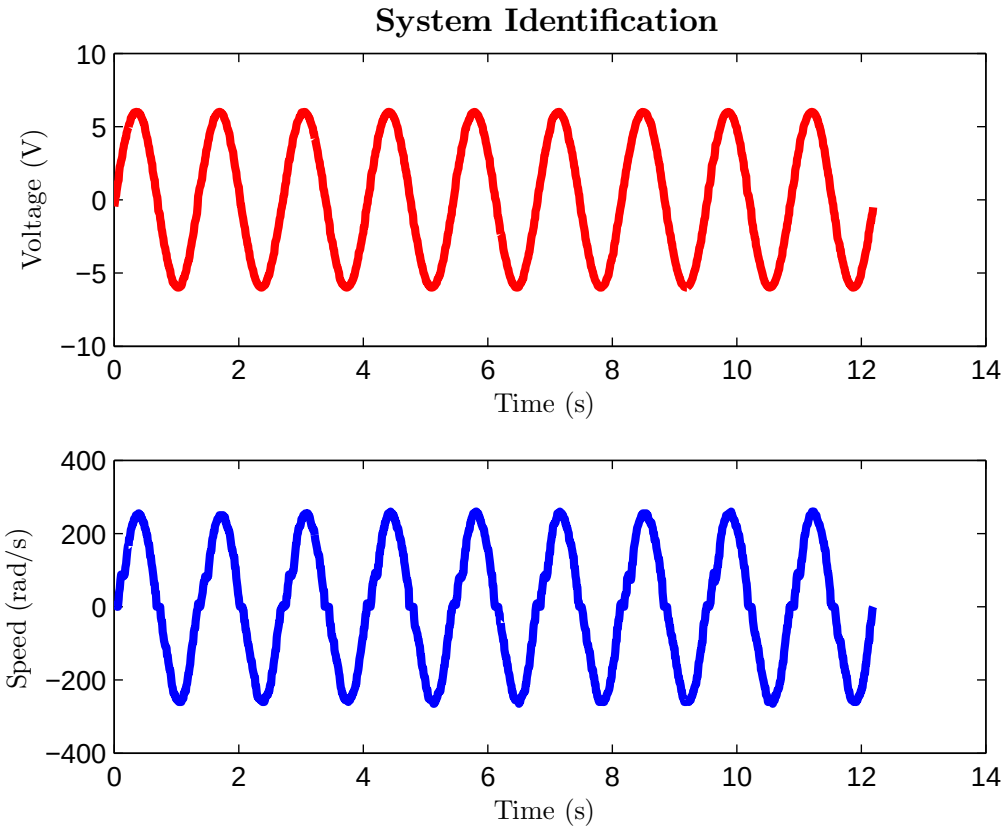

Fig. 3.6.: Sample input (voltage) and output (speed) data given to the MATLAB system identification toolbox.

Table 3.2: Summary of the results for the identification experiments used to estimate the first-order transfer function parameters of the transmission mechanisms w.r.t DC motor joints from the speed and voltage data.

Motor Joint	Virtual Inertia	Virtual Friction
Swing Knee	4.4 E-4	0.026
Swing Hip	12.3 E-4	0.026
Stance Hip	2.74 E-4	0.024
Stance Knee	4.26 E-4	0.025

3.2.1 Construction of Voltage Trajectories

Using the speed and acceleration data from simulation, J_v and B_v from identification experiments, voltage trajectories for a single step of a robot are constructed

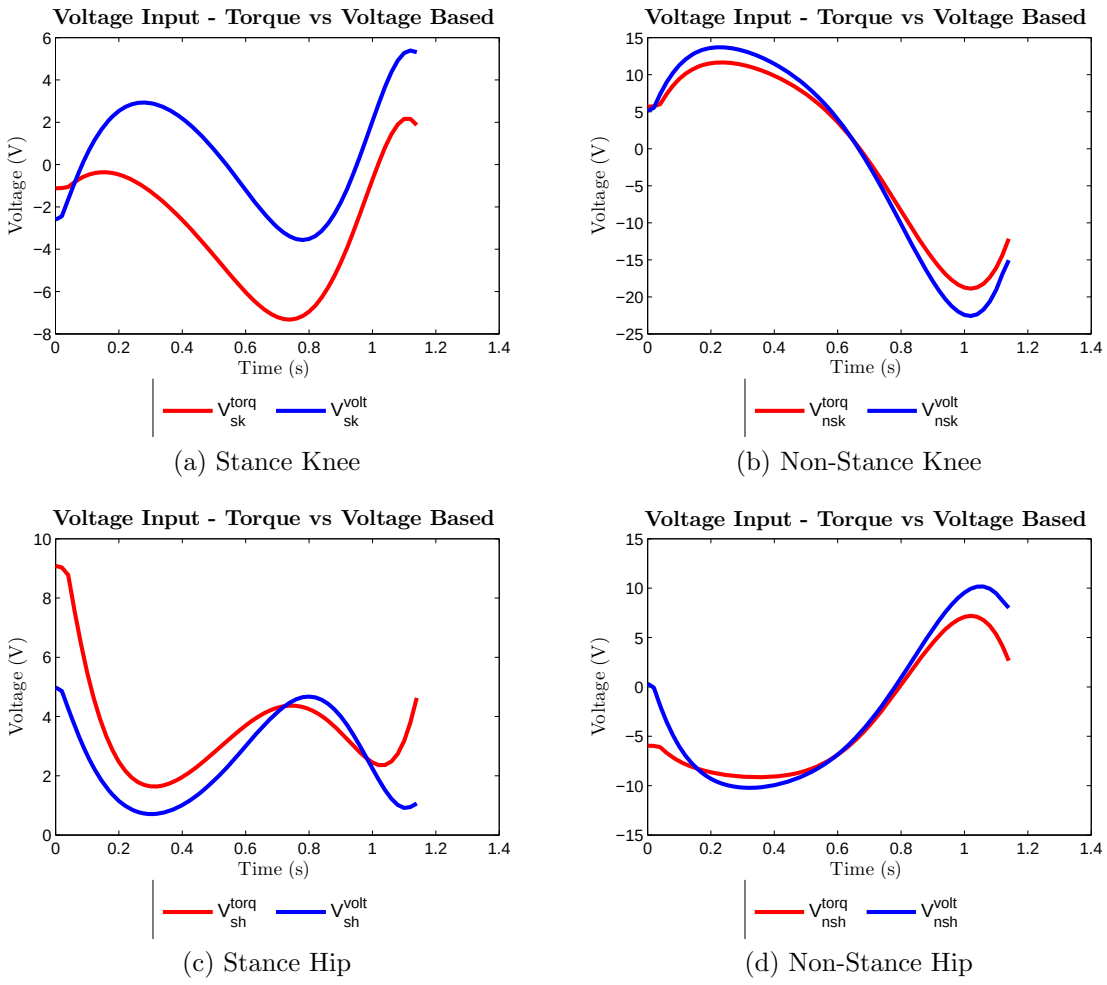

(a) Stance Knee (b) Non-Stance Knee

(c) Stance Hip (d) Non-Stance Hip

Fig. 3.7.: Torque-based vs. Voltage-based input trajectories for one step: constructed using the values of speed, acceleration and torque from the simulation walking data for AMBER (Fig. 3.1).

for all the joints using V4. Utilizing the simulated torque (u) and speed data, the equivalent voltage profiles are generated using V6.

$$V_{in} = (u/k_{\varphi})r_a + k_{\omega}\omega \tag{V6}$$

Hence for a given walking gait (Fig. 3.1), the voltage trajectories that would be needed in the case of a traditional torque-based control and a direct voltage-based

control using identification data, display a close agreement for a DC motor model with negligible inductance as seen in Fig. 3.7.

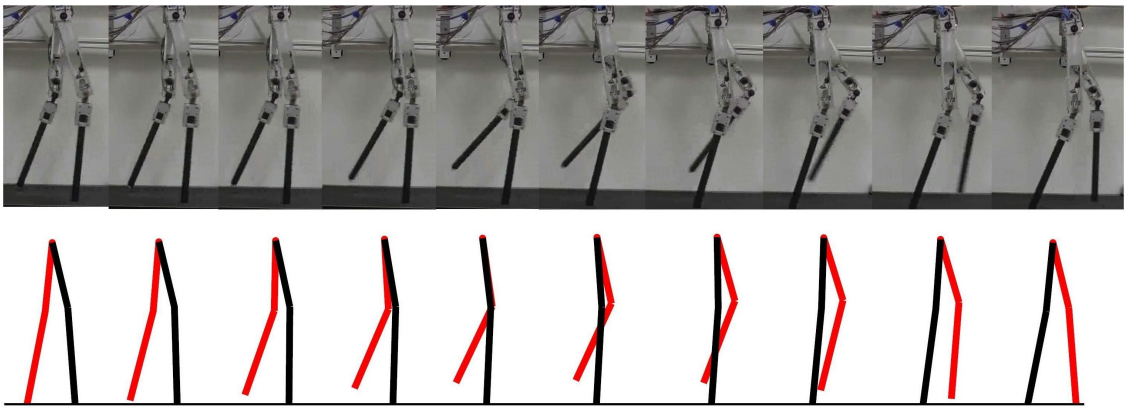

Fig. 3.8.: Walking tile of AMBER: experiment gait obtained by directly feeding the voltage-based profiles (as seen in Fig. 3.7) to DC motors vs simulation gait obtained using input/output linearization on outputs obtained from human-inspired optimization (Fig. 3.1).

Hence, this experimental procedure serves as a foundation for the utility of a direct voltage-based approach for the control of AMBER instead of a torque-based approach. With AMBER suspended using a rope with marginal foot contact with the ground and feeding these time-based voltage profiles directly to the DC motor drives, the robot displayed a walking motion which is similar to the simulated walking (see Fig. 3.8). This was a good indication of the applicability of direct voltage-based control approach for continuous dynamics behavior. But bipeds are hybrid control systems and have a discrete dynamics during foot impacts, so by devising a voltage-based approach which incorporates the configuration of the robot with discrete dynamics behavior, it could potentially result in walking. This line of thought provided the idea for using voltage-based proportional control on the outputs which are hybrid zero dynamics compliant for experimental implementation on AMBER.

4. VOLTAGE-BASED P-CONTROL IMPLEMENTATION ON AMBER

The control law (2.10) used for human-inspired control simulation, linearizes the dynamics of AMBER through model inversion, which requires exact values of masses, inertias and dimensions of the robot. This is not only complex to implement but realizing it on AMBER could potentially consume both time and resources, and achieving walking may still not be guaranteed due to a potentially inexact model. Therefore, a different approach is considered by arguing that due to the "correct" choice of output functions—and specifically the human-inspired outputs—it is possible to obtain walking through simple controllers that are easy to implement and inherently more robust. Specifically, a voltage-based proportional controller on the human-inspired outputs is presented, and it was verified through simulation that robotic walking is obtained on AMBER. The simplicity of this controller implies that it can be efficiently implemented in software, and the details of this implementation are presented in this chapter, followed by the experimental results, which show that "human-like" bipedal robotic walking could be obtained on AMBER that is both efficient and robust.

4.1 Human-Inspired Voltage Control

Even if walking is obtained formally through input/output linearization, i.e., model inversion, the controllers are often implemented through PD control on the torque (see, for example, [32]). Since AMBER is not equipped with torque sensors, an alternative method for feedback control implementation is considered. Because AMBER is powered by DC motors, the natural input to consider is voltage, V_{in}, which indirectly affects the torques acting on the joints. Let V_{nsl}, V_{sk}, V_{nsk} and V_{tor} be the voltage input to the motors at the non-stance hip, stance knee, non-stance

knee and stance hip, respectively. Define the following human-inspired proportional (P) voltage control law:

$$V_{in} = \begin{bmatrix} V_{nsl}(\theta) \\ V_{sk}(\theta) \\ V_{nsk}(\theta) \\ V_{tor}(\theta) \end{bmatrix} = -K_p y_\alpha(\theta), \tag{4.1}$$

where K_p is the constant matrix with its diagonal entries being the proportional gain of 1.75 for each of the motors and its non-diagonal entries are zero since the motors are controlled independently. This controller can be applied to the control system $\dot{x} = f_{R_v}(x) + g_{R_v}(x)V_{in}$ modeling the bipedal robot in conjunction with the motors. It can be seen that the control law (proportional control) solely depends on the generalized coordinates of robot (angles), θ, and not on the angular velocities. This marks a drastic change from the traditional ways of computing control. Evidently, and importantly, this avoids computation of angular velocities of the joints, which would have been computationally expensive and inaccurate.

It is important to note that the voltage-based P-controller (4.1) is equivalent to a PD torque controller, where the derivative (D) constant is specified by the properties of the motor:

$$V_{in} = -K_p y_\alpha(\theta) = R_a i_a + K_\omega \omega \implies u(\theta, \dot{\theta}) = -K_\varphi R_a^{-1} K_p y_\alpha(\theta) - K_\varphi R_a^{-1} K_\omega \dot{\theta}$$

where K_φ is the torque constant matrix, and K_ω is the motor constant matrix. Hence, the control being applied is, in the end, related to the conventional torque PD control methods adopted in literature (see [50]). Fig. 3.7 supports this analytical observation of similarity between torque-based PD control and voltage-based P-control, for a DC motor with inductance neglected.

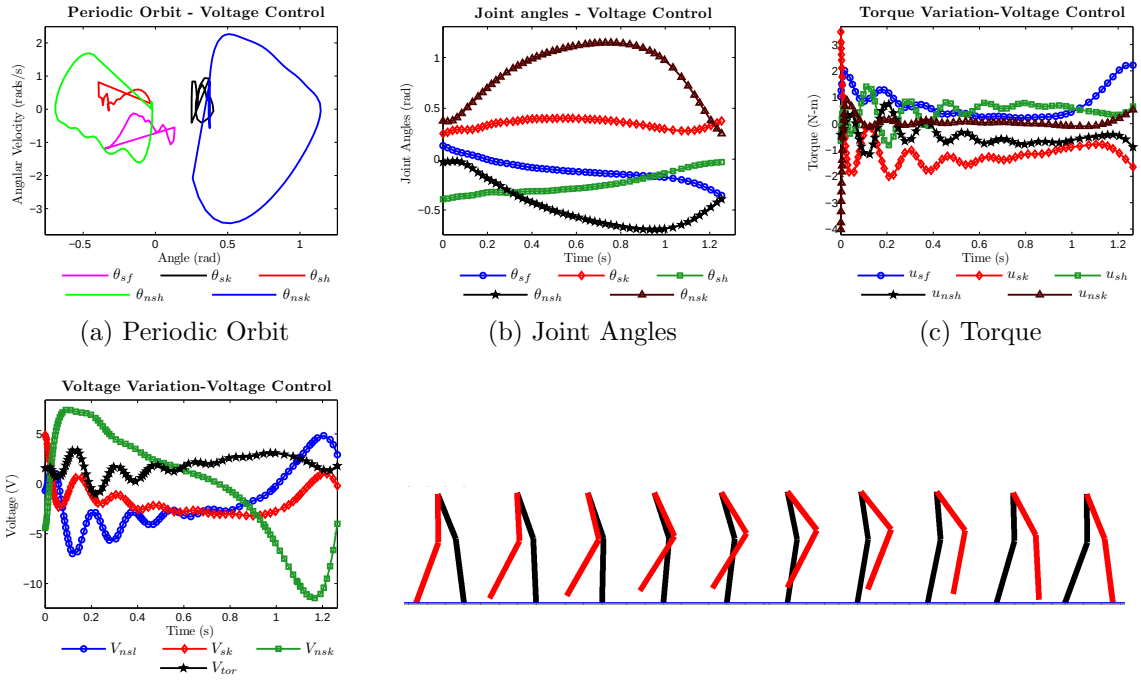

(a) Periodic Orbit (b) Joint Angles (c) Torque

(d) Voltage (e) Tiles of the Walking Gait. See video: [52]

Fig. 4.1.: Walking gait for AMBER obtained in simulation through P-voltage control.

4.2 Simulation Results

To obtain walking in simulation with AMBER using P-control on outputs, hybrid model $\mathscr{HC}_R$ of the robot is constructed which is given by (2.1). Applying the human-inspired controller (2.10) and solving the optimization problem subject to the additional constraints results in a hybrid system $\mathscr{H}_R^{(\alpha^*,\varepsilon)}$ that provably has a stable periodic orbit, i.e., a stable walking gait. The parameters α^* are then used in the voltage-based P-control, and the resulting closed loop system, which includes the mechanical and electrical models of AMBER is simulated. This results in a new periodic orbit (that is "near" the periodic orbit for the human-inspired torque controller). The resulting walking that is obtained through P-control is shown in Fig. 4.1, along with the periodic orbit, joint angles, torques and voltages.

4.3 Experimental Implementation and Results

AMBER's experimental set up consists of three main segments- controller, actuators and sensors. Controller is implemented using LabVIEW Real Time (RT) and FPGA. Real Time Processor is used for floating point operations, while FPGA interacts with I/O devices, provides parallel execution and silicon hardware level speed of nanosecond operations for time critical logic, which makes the combination of RT and FPGA ideal for controlling a complex machine like a biped. DC motors are used to actuate all the joints of the robot, with absolute encoders on all joints, torso and contact switches at foot ends providing sensing mechanisms used to implement feedback control law. The biped is powered from an off-board power supply and all interconnections are established through wires. Before the experiment is started, the treadmill speed (resolution of 0.1 mph) is adjusted to be roughly equal to the desired average speed of walking (0.8 mph) and then the speed is fine tuned using an autotransformer which changes the supply voltage to treadmill. In this manner, the net effect of the walking is close to the flat ground walking. The robot is then powered on and slowly lowered down to the treadmill, after couple of steps, the robot steadily falls into a limit cycle to achieve robust walking. Before the experiment is stopped, the robot is held by the experimenter to avoid it falling on the ground and then lifted off the treadmill. Protection scheme is implemented for AMBER upon detection of undesired behavior, when the encoder fails (or) when joint angles fall out of prescribed range of motion, the robot is powered off.

Table 4.1 gives the list of components used and specifications associated with each of them and Fig. 2.1 gives the the locations of various sensors and actuators on biped, since the robot is symmetrical, locations are highlighted on only one of the legs. The rest of this section is devoted to explaining control law implementation algorithms, control of DC motor, angle calculation using absolute encoder, guard detection using foot switch and finally the results of AMBER walking are presented.

Table 4.1: Summary of the components used for bipedal walking with AMBER.

Component	Manufacturer	Model Number	Specifications
DC Motor	Maxon	222052	11W, 18V
Gear	Maxon	143989	157:1
Absolute Encoder	US Digital	MAE3	4096 counts/rev
Contact Switch	Honeywell	AML21CBA2BA	SPDT
Real Time Controller	NI	cRIO 9024	800 MHz, 512 MB DRAM
Chassis	NI	cRIO 9114	8-Slot,Virtex5-LX50 FPGA
DC Motor Drive	NI	NI 9505	24V
Power Supply	NI	NI PS 16	24V,10A
Treadmill	TreadDesk	The Tread	0.5 mph-4 mph

4.4 Implementation of Feedback Control Law

Overview of the implementation of voltage based P-control on human-inspired outputs for AMBER is presented in Fig. 4.2. This section presents the algorithmic implementation for each module in the form of flowcharts. Fig. 4.3 presents the architectural overview of interaction between controller modules and data logging module. Data Logging is performed using network published variables. They stream the data between the Host PC (Fig. 4.4) and RT using a 100ms thread via an ethernet connection. Host PC has file I/O, hence it is used to store joint angles and voltage data used for control law implementation. Control law is implemented across both LabVIEW - RT (Fig. 4.5) and FPGA (Fig. 4.6) modules. From the FPGA resource utilization summary (39%) and total power consumption per step (27 W), it is evident that the control law is not resource intensive for implementation purposes. This highlights the effectiveness and simplicity of the algorithm used to implement the control law and this is potentially one of the reasons why the walking obtained was so robust.

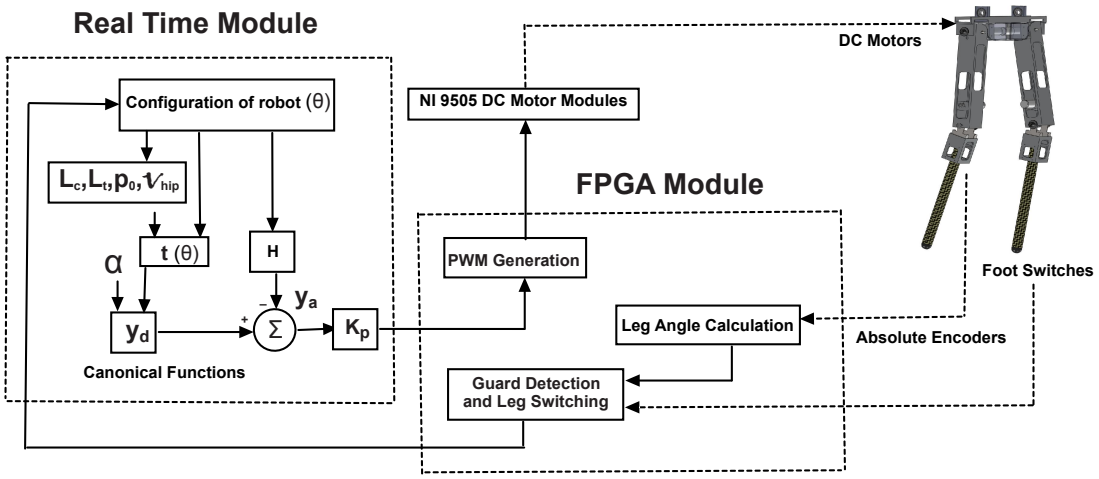

Fig. 4.2.: Schematic of experimental implementation of the voltage-based proportional controller on the human-inspired outputs.

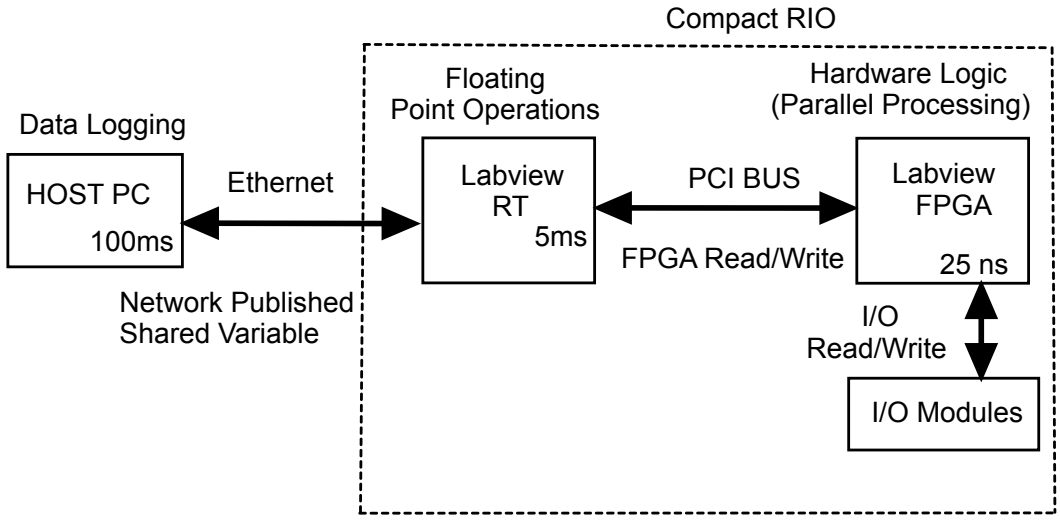

Fig. 4.3.: Overview of the functional behaviour with interface protocols used between Host, RT and FPGA LabVIEW modules.

4.4.1 Brushed DC Motor Control

Pulsed Width Modulation (PWM) technique is used to control the voltage applied to the brushed DC motor, which effectively controls the torque and speed of DC

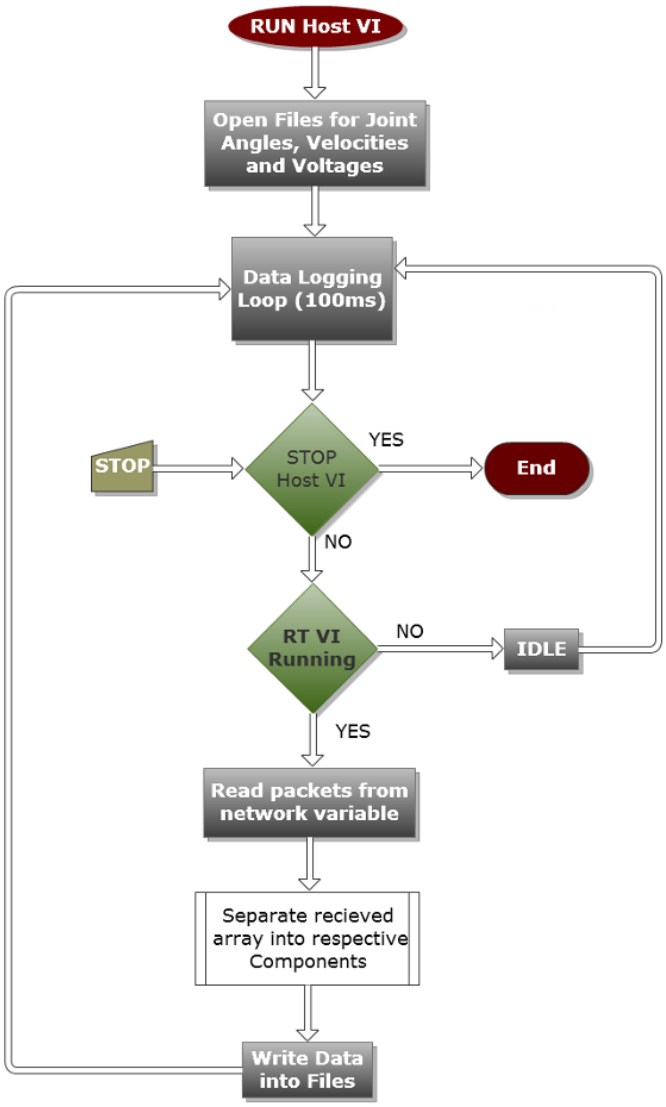

Fig. 4.4.: Flowchart representation of the Host algorithm.

motor operation. Resistance of motor (6.44 Ω) is large when compared to inductance (0.309 mH), hence it was possible to implement a P-control, since the dynamics of current can be ignored. The control law which is depicted in Fig. 4.2, produces PWM count equivalent to the duty cycle of the PWM pulse i.e., voltage that needs to be applied to the motor. Then, the FPGA generates a PWM pulse which will be given to NI 9505 DC motor module and the sign of the PWM count specifies the drive

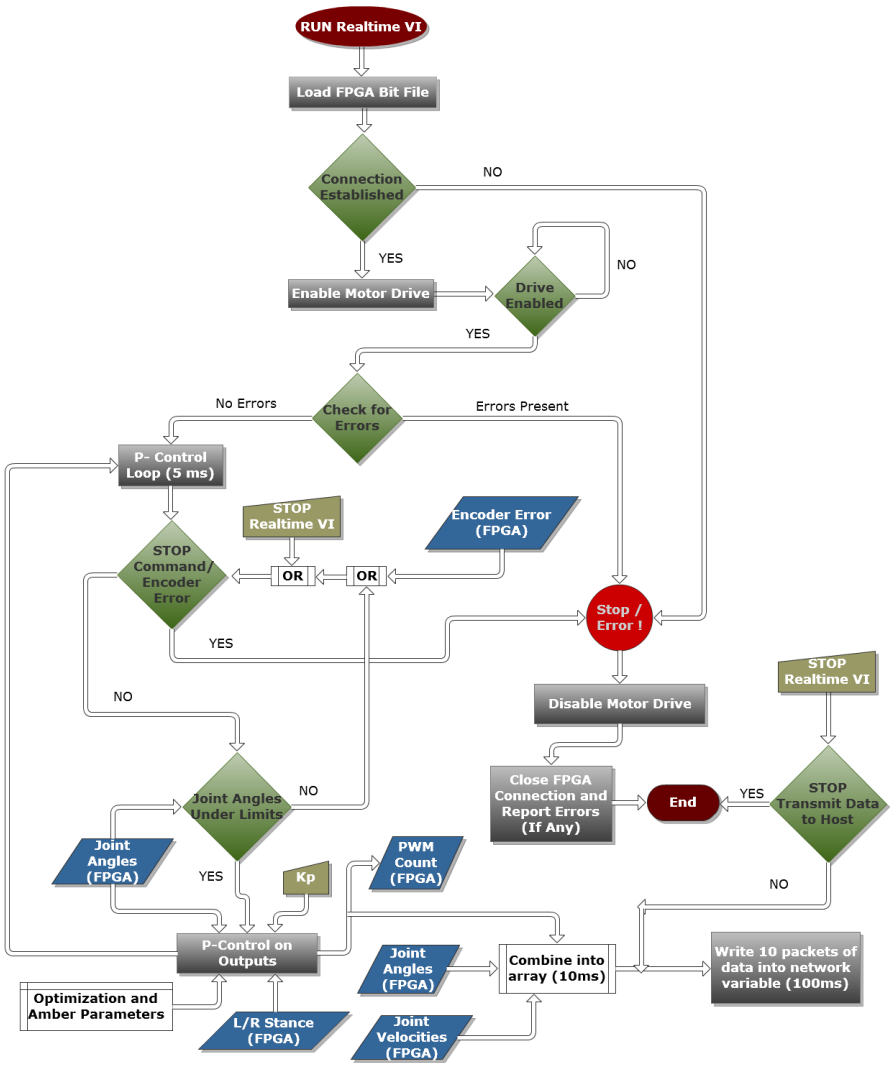

Fig. 4.5.: Flowchart representation of the LabVIEW RT algorithm.

direction (see Fig. 4.7). The H-bridge controller inside NI 9505 module operates at 20 KHz, while the FPGA operates at 40 MHz which corresponds to 2000 FPGA clock tick counts. Since the motor is rated at 18 V and module can supply 24 V, the maximum duty cycle is limited to 75%. There is a minimum restriction of pulse width of 2 μs, this results in a usable duty cycle range of 4% to 75% for the control of DC motor.

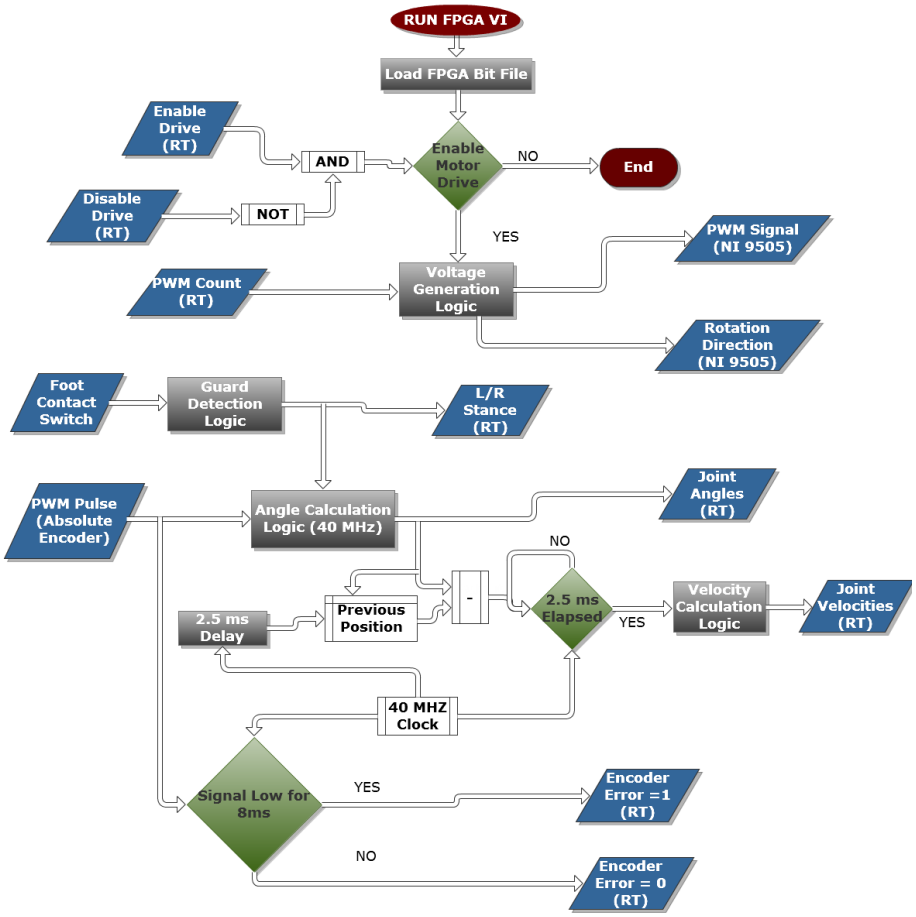

Fig. 4.6.: Flowchart representation of the LabVIEW FPGA algorithm.

4.4.2 Absolute Encoder Logic and Operation

Absolute encoder sends a PWM pulse to NI 9505 module with pulse width proportional to the angle of rotation (see Fig. A.2b). The scaling factor that is used to calculate the angles for various joints from the encoder pulses can be obtained from the data sheet.

In short, 4097 μs of encoder pulse width is equivalent to 2π radians of one complete rotation. By using 40 MHz clock to sample this encoder pulse (1 FPGA count = 0.025 μs) as shown in Fig. 4.8, we get 163880 counts for every rotation, which results in 26082 counts/radian. Hence by determining the counts registered, angle of

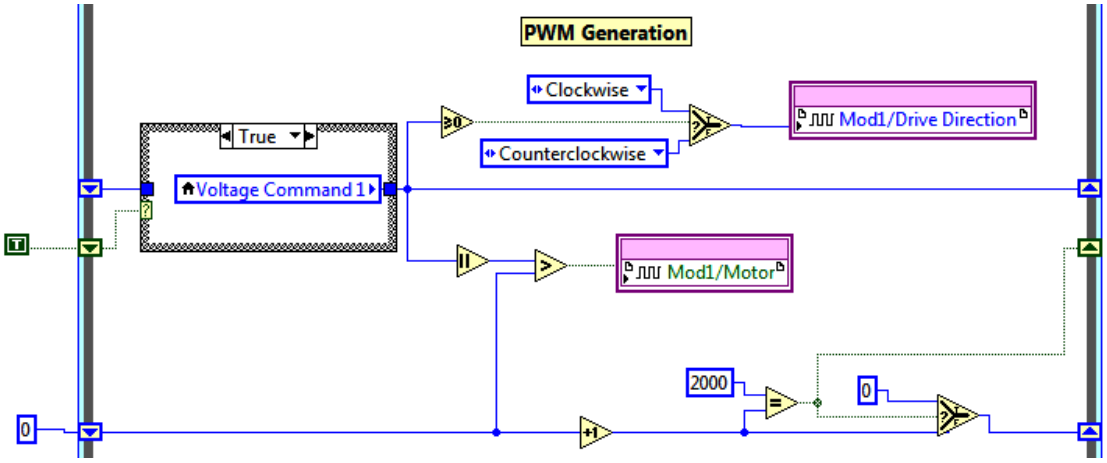

Fig. 4.7.: Schematic for the generation of PWM signal for DC motor control in LabVIEW FPGA.

a joint is calculated. Encoder calibration is done prior to starting of the experiment to determine the zero degree position for every joint, relative to which all angles of that respective joint are calculated during the experiment. Protection is built into the system based on encoder values, the motors will be powered down when any of encoder doesn't work (or) range of motion on any of joints exceeds the set limits.

4.4.3 Pushbutton Contact Switches Operation

The pushbutton switches are used at the end of each foot, they are Single Pole Double Throw (SPDT) type. So when the button is in pressed position it sends a Logic 0 to FPGA, when it is in relaxed position it sends a Logic 1. The FPGA logic that is used to detect the guard and initiate the switching of legs is shown in Fig.4.9 .The following variable- L/R stance is used for to keep track of which leg is stance leg. So when left leg is stance leg, the watchdog in the controller looks every 5 ms to see whether right leg hit the guard and vice versa, when the right leg is in stance position. Debounce logic for 0.2 s is implemented, which discards any swing leg

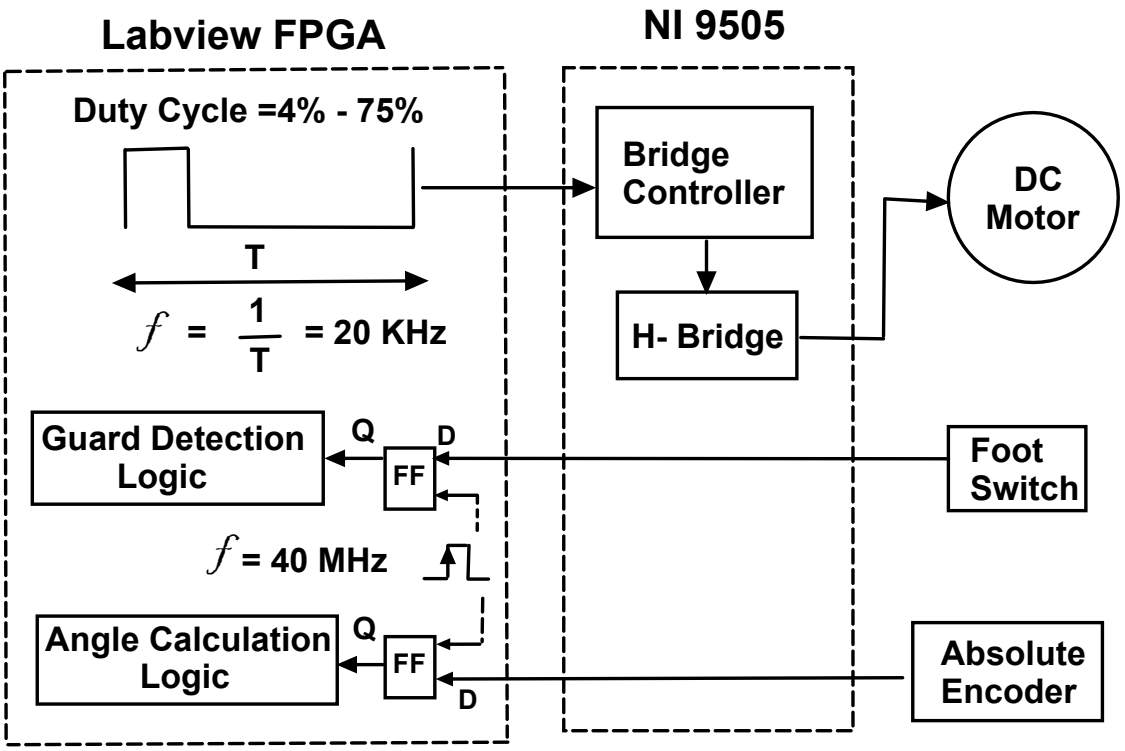

Fig. 4.8.: I/O operations with FPGA level processing, timing and hardware interconnection diagram.

contact happening in less than 0.2 s from the previous guard. Hence this debounce logic eliminates false steps where swing leg hits the ground behind the stance leg.

4.5 Results

Implementing the proposed voltage-based P-controller on AMBER, results in bipedal robotic walking (see [53] for a video of AMBER walking and responding to external disturbances). Fig. 4.10 presents the summary of the resource utilization for the controller implementation on AMBER. Walking tiles for the experimental walking obtained on AMBER using this control scheme is shown in the Fig. 4.11, where they are compared against the simulated walking behavior. The similarity between the experimental and simulated behavior can be further seen by by compar-

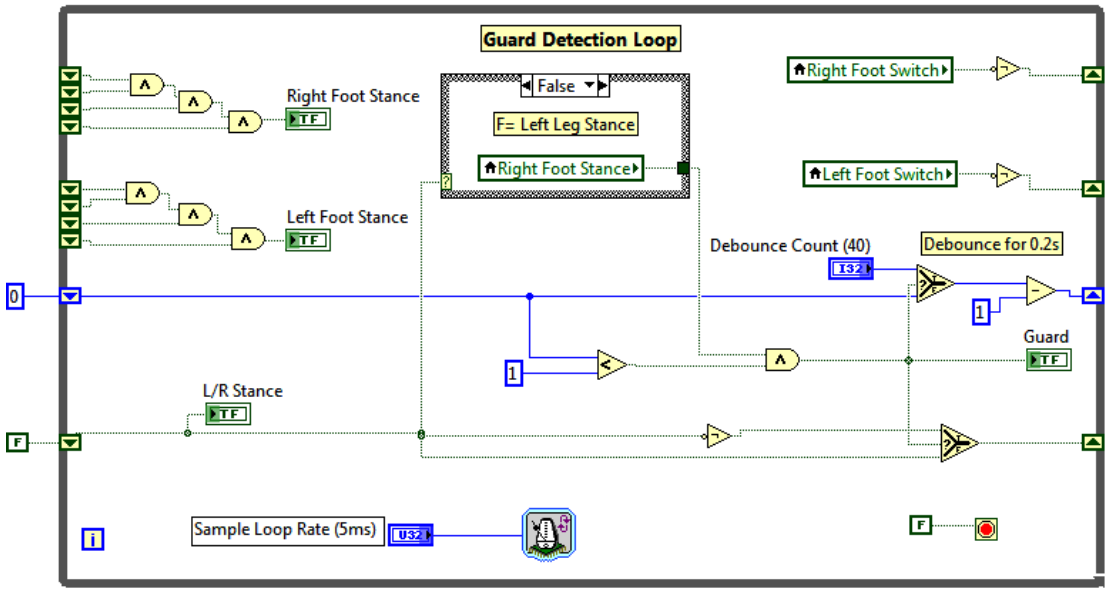

Fig. 4.9.: LabVIEW FPGA implementation of guard detection with debounce logic for 0.2 seconds.

ing the joint angles predicted in simulation and the joint angles seen experimentally. Even though there is no direct control on angles, as shown in Fig. 4.12, owing to the controller driving the actual outputs of robot to the desired outputs, angle tracking displays a very good matching with the simulated gait. Due to the human-inspiration for the controller design, the walking achieved by AMBER is efficient, robust and "human-like." The specific cost of transport (electrical) for AMBER walking at 0.44 m/s is 1.88 using an average power of roughly 27 W, which is very low compared to commercial robots like Honda [11] and it also has the least installed power to weight ratio (W/Kg) among the robots with no compliance as indicated in Table 4.2, which is a critical aspect in reduction of total cost of equipment by reducing the size of motors and the rating of power supplies. In addition, the walking achieved with AMBER is incredibly robust; with no changes to the controller, AMBER can successfully navigate over rough terrains with ease (a video of this can be found at [42]). Finally, on comparison of the outputs observed on AMBER to the human output

data from which the controller was originally derived (see Fig. 4.13), demonstrates that the walking is remarkably "human-like" despite the vast differences between AMBER and a human.

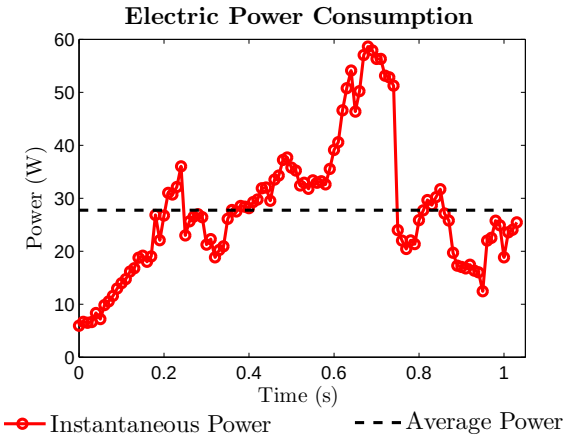

(a)

Component	Total	Used (%)
Slices	7200	39
Slice Registers	28800	20.8
Slice LUTs	28800	28.1
DSP48s	48	20.8
Block RAMs	48	0

(b)

Fig. 4.10.: (a.) Plot representing the values of instantaneous and average power consumed by AMBER over a single step. (b.) Summary of FPGA device utilization after post-synthesis mapping [54].

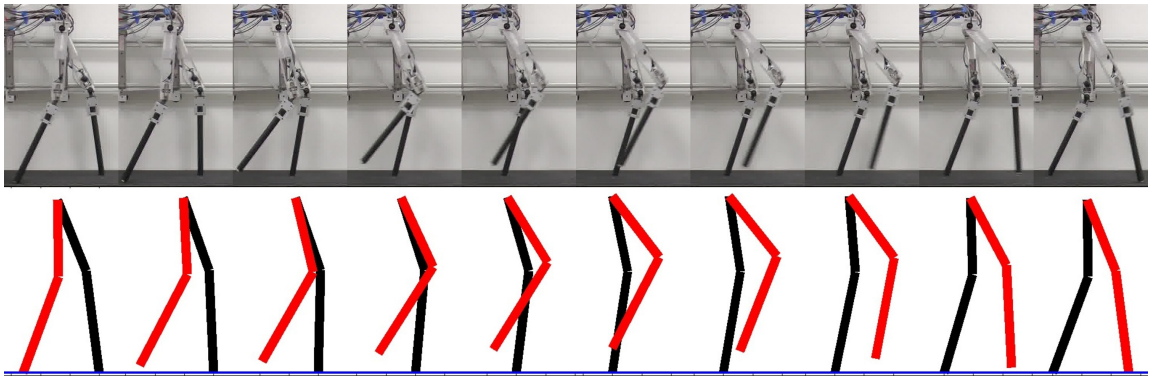

Fig. 4.11.: Walking tile of AMBER experiment vs simulation for one step using voltage-based P-control (see video at [53]).

Table 4.2: Comparison of installed power to weight ratio (W/Kg) of AMBER with contemporary bipedal robots.

Robot	Compliance	Value	Reference
AMBER	No	13.2	44W, 3.33kg
ERNIE	Yes	53.7	1 KW[1], 18.6kg [19]
RABBIT	No	93.2	2.98 KW[2], 32kg [19]
NAO H25 V3.3	No	35.4	177W[3], 5kg [55]
DARWIN	No	27.6	80W[4], 2.9kg [56]
MABEL	Yes	58.6	3.28 KW[5], 56kg [50]
Cornell Biped	Yes	1.5	19W[6], 12.7kg [11]

[1] EC 45-136212 (250 W) , so for 4 motors total power= 1 KW

[2] RS 420J performace curves indicate 1 HP motor, so for 4 motors total power= 2.98 KW

[3] Type1: RE-MAX 17 (4W), Type2: RE-MAX 24 (11W). Type1 Motors on Head-2 , Type1 Motors on Arms -12 , Type2 Motors on Legs- 11. Total power for 25 motors = 177W

[4] Specifications of Dynamixel RX-28 at 12 V has values of RE-MAX 17 motor(4W) with 1:193 gear ratio, so for 20 motor modules total power= 80 W

[5] QBO5600-X0X (843.892 W)- 2 ,QBO5601-X0X(798.605 W) - 2 , so for 4 motors total power= 3.28 KW

[6] For two 9.5 Watt 6.4 oz MicroMotors, total power= 19 W

4.6 Subject to Uneven Terrain: Robust Walking

In order to verify the robustness of the walking obtained from the flat-ground optimization i.e., by implementing P-control using α^*, the biped is made to walk on rough terrain with a change of 1.94 cm in terrain height by placing wooden blocks in the walking path of the robot and AMBER could compensate the changes in terrain and recover the normal walking gait after overcoming the disturbance, as can be seen in Fig. 4.14, and the walking video with AMBER responding to wide array of disturbances is available at [53].

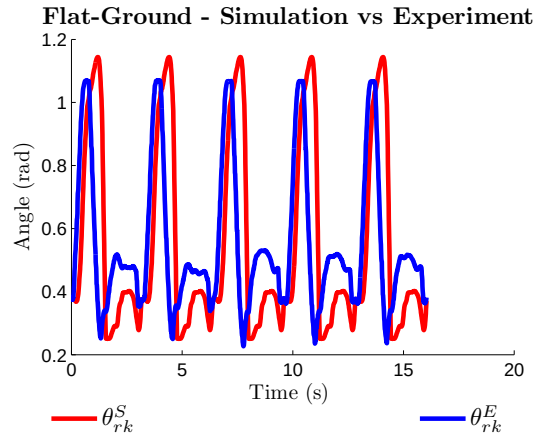

(a) Stance Knee Trajectory

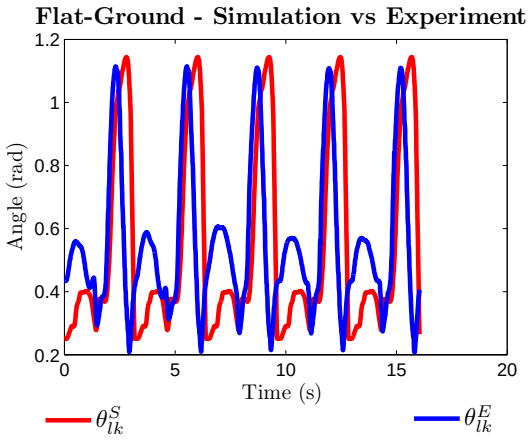

(b) Non-Stance Knee Trajectory

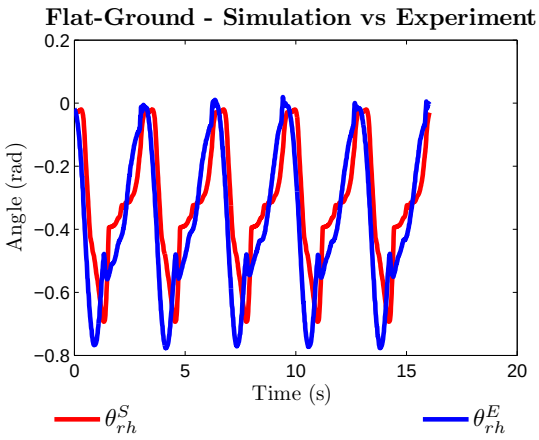

(c) Stance Hip Trajectory

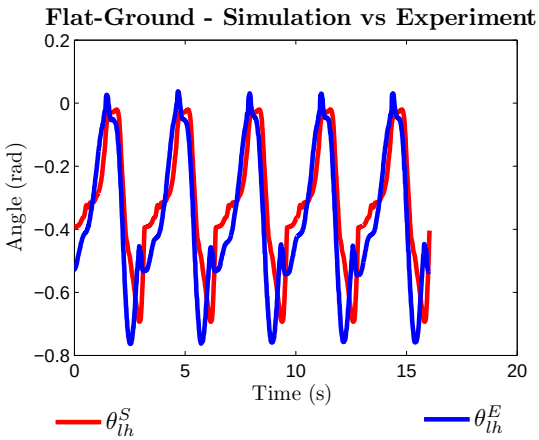

(d) Non-Stance Hip Trajectory

Fig. 4.12.: Experimental vs simulation data for 10 walking steps of AMBER using P-Control: blue lines indicate the experimental values for the joint angles, while the red lines indicate the joint angles for the simulation.

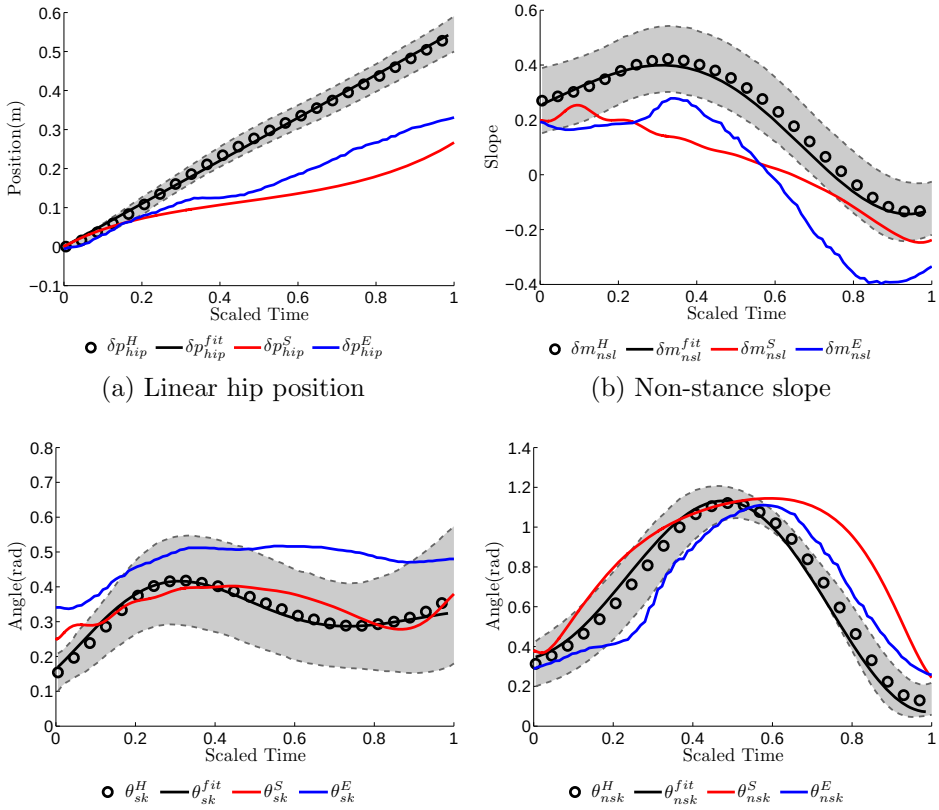

(a) Linear hip position (b) Non-stance slope

(c) Stance Knee (d) Non-stance Knee

Fig. 4.13.: Mean of the trajectories of the human outputs from all test subjects put together are plotted in here. The grey shaded area indicate the standard deviation from the mean trajectory. The black lines are the fits of the canonical functions to the mean human data. Red lines are human-inspired optimization fits of walking functions for AMBER with constraints in simulation. Blue lines correspond to the experimental values of the actual outputs of AMBER during walking.

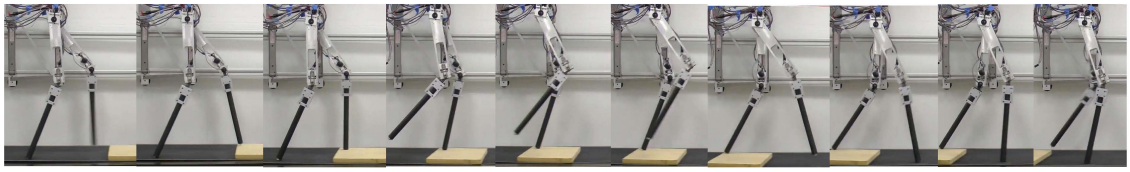

Fig. 4.14.: Tile of AMBER walking over an obstacle of 1.94 cm and recovering the walking gait with voltage-based P-control.

5. CONCLUSIONS AND FUTURE CHALLENGES

This thesis work successfully translated formal methods in human-inspired control to efficient algorithmic implementation and, finally, experimentally realized walking on AMBER. Specifically, identification experiments were presented that form the foundation for voltage-based P-control approach for obtaining walking on AMBER. The simplicity of the algorithmic implementation of this control law resulted in low computation overhead, time step of 5ms for each calculation, and minimal hardware resources (39% of the FPGA). With no actuation at ankles, the overall energy efficiency is enhanced, which enabled AMBER to have the lowest installed W/Kg when compared with the contemporary robots, as shown in Table 4.2. While it must be pointed out that some of the robots also carry support electronics which has resulted in them having higher power requirement, the proposed method of voltage-based P-control on human-inspired outputs can result in robust walking with a very good cost of transport. While achieving a walking gait that is very close to the natural human walking gait, the biped is also tolerant to changes in terrain (6cm), change of treadmill speeds (12.5%) and even force disturbances on all of the links of the robot. It must be highlighted that the proposed voltage-based control law is dependent only on the configuration variables as opposed to using speed and current feedback, and this constitutes the inherent simplicity and advantage of indirectly affecting the torque produced at a joint. This simplicity results in robust walking both in simulation as well as in the experiment.

Future challenges include but are not limited to implementing motion primitives: walking at multiple speeds, start/stop of the robot, walking up/down stairs and running, with smooth transitions between each of the modes. Building compliance into the rigid robot structure with implementation of ankle control and foot placement will be a good addition, as it would result in more anthropomorphic appearance with improved energy efficiency. The next research step would be to transfer the

ideas used for 2D walking to implement 3D bipedal robotic walking and running using human-inspired control techniques for the design of prosthetic legs, with the ultimate goal of helping humans with lower limb amputation to gain their natural walking gait.

REFERENCES

[1] M. Y. Zarrugh and C. W. Radcliffe, "Computer generation of human gait kinematics," *Journal of Biomechanics*, vol. 12, no. 2, pp. 99–111, 1979.

[2] A. S. McIntosh, K. T. Beatty, L. N. Dwan, and D. R. Vickers, "Gait dynamics on an inclined walkway," *Journal of Biomechanics*, vol. 39, no. 13, pp. 2491–2502, 2006.

[3] B. J. McFadyen and D. A. Winter, "An integrated biomechanical analysis of normal stair ascent and descent," *Journal of Biomechanics*, vol. 21, no. 9, pp. 733–744, 1988.

[4] D. P. Stephen, N. H. Erika, J. G. Jennifer, and S. F. James, "Locomotor adaptations for changes in the slope of the walking surface," *Gait & Posture*, vol. 20, no. 3, pp. 255–265, 2004.

[5] A. J. Ijspeert, "Central pattern generators for locomotion control in animals and robots: a review," *Neural Networks*, vol. 21, no. 4, pp. 642–653, May 2008.

[6] J. Bo. Nielsen, "How We Walk: Central Control of Muscle Activity during Human Walking," *The Neuroscientist*, vol. 9, no. 3, pp. 195–204, 2003.

[7] I. Yu and W. Yu, "The Roles of CPG Phase Modulation and Reflexive Muscular Patterns in Balance Recovery Reflexive Responses to Perturbation during Walking - A Simulation Study," in *29th Annual International Conference of the IEEE Engineering in Medicine and Biology Society*, pp. 2389-2392, 22-26 Aug. 2007.

[8] A. N. Lay, C. J. Hass and R. J. Gregor, "The effects of sloped surfaces on locomotion: A kinematic and kinetic analysis," *Journal of Biomechanics*, vol. 39, no. 9, pp. 1621–1628, 2006.

[9] M. H. Raibert, "Legged Robots," *Communications of the ACM*, vol. 29, no. 6, pp. 499–514, Jun. 1986.

[10] T. McGeer, "Passive Dynamic Walking," *International Journal of Robotics Research*, vol. 9, no. 2, pp. 62–82, Apr. 1990.

[11] S. Collins, A. Ruina, R. Tedrake, and M. Wisse, "Efficient Bipedal Robots Based on Passive-Dynamic Walkers," *Science*, vol. 307, no. 5712, pp. 1082–1085, Feb. 2005.

[12] M. W. Spong, "Passivity Based Control Of The Compass Gait Biped," in *Proc. of IFAC World Congress*, Beijing, China, pp. 19–24, 5-9 Jul. 1999.

[13] P. Holmes, R. J. Full, D. Koditschek, and J. Guckenheimer, "The Dynamics of Legged Locomotion: Models, Analyses, and Challenges," *SIAM Rev.*, vol. 48, no. 2, pp. 207–304, Feb. 2006.

[14] I. Poulakakis and J. W. Grizzle, "The Spring Loaded Inverted Pendulum as the Hybrid Zero Dynamics of an Asymmetric Hopper," *IEEE Transactions on Automatic Control*, vol. 54, no. 8, pp. 1779–1793, 2009.

[15] H. Geyer, A. Seyfarth and R. Blickhan,"Compliant leg behaviour explains basic dynamics of walking and running," *Proceedings of the Royal Society B: Biological Sciences*, vol. 273, no. 1603, pp. 2861–2867, Nov. 2006.

[16] H. Geyer and H. Herr,"A Muscle-Reflex Model That Encodes Principles of Legged Mechanics Produces Human Walking Dynamics and Muscle Activities," *IEEE Transactions on Neural Systems and Rehabilitation Engineering*, vol. 18, no. 3, pp. 263–273, Jun. 2010.

[17] S. Srinivasan, I. A. Raptis and E. R. Westervelt,"Low-Dimensional Sagittal Plane Model of Normal Human Walking," *ASME Journal of Biomechanical Eng.*, vol. 130, no. 5, p. 051017, Oct. 2008.

[18] U. Mettin, P. La Hera, L. Freidovich, A. Shiriaev, and J. Helbo,"Motion Planning for Humanoid Robots Based on Virtual Constraints Extracted from Recorded Human Movements," *Intelligent Service Robotics*, vol. 1, no. 4, pp. 289–301, 2008.

[19] E. R. Westervelt, J. W. Grizzle, C. Chevallereau, J. H. Choi, and B. Morris, *Feedback Control of Dynamic Bipedal Robot Locomotion*. Boca Raton: CRC Press, Jun. 2007.

[20] I. R. Manchester, U. Mettin, F. Iida, and R. Tedrake, "Stable dynamic walking over uneven terrain," *International Journal of Robotics Research*, vol. 30, no. 3, pp. 265–279, Mar. 2011.

[21] S. Kajita and K. Tani, "Experimental study of biped dynamic walking," *Control Systems, IEEE*, vol. 16, no. 1, pp. 13–19, Feb. 1996.

[22] J. K. Hodgins and M. N. Raibert, "Adjusting step length for rough terrain locomotion," *IEEE Transactions on Robotics and Automation*, vol. 7, no. 3, pp. 289–298, Jun. 1991.

[23] J. Kim, I. Park and J. Oh, "Walking Control Algorithm of Biped Humanoid Robot on Uneven and Inclined Floor," *Journal of Intelligent and Robotics Systems*, vol. 48, no. 4, pp. 457–484, Apr. 2007.

[24] Z. Qiu-Bo, P. Song-Hao and G. Chao, "Motion planning for humanoid robot based on hybrid evolutionary algorithm," *International Journal of Advanced Robotic Systems*, vol. 7, no. 3, pp. 209–216, 2010.

[25] C. Zhou, P. K. Yue, J. Ni, and S. Chan, "Dynamically stable gait planning for a humanoid robot to climb sloping surface," in *IEEE Conference on Robotics, Automation and Mechatronics*, vol. 1, pp. 341–346, 1-3 Dec. 2004.

[26] J. Lin, J. Chang, S. M. Lyu, S. W. Wang, and Y. W. Lin, "Locomotion control of a biped robot for stair-climbing by fuzzy stabilization tuning approach," in *IEEE International Conference on Control Applications*, pp. 1590–1595, 8-10 Sep. 2010.

[27] Q. Wang, Y. Huang, J. Zhu, B. Chen, and L. Wang, "Dynamic walking on uneven terrains with passivity-based bipedal robots," in *Lecture Notes in Electrical Engineering: Informatics in Control Automation and Robotics*, vol. 85, pp. 187–199, Springer Berlin Heidelberg, 2011.

[28] Y. F. Zheng and J. Shen, "Gait synthesis for the SD-2 biped robot to climb sloping surface," *IEEE Transactions on Robotics and Automation*, vol. 5, no. 1, pp. 86–96, Feb. 1990.

[29] S. Ching-Long, "Ascending and descending stairs for a biped robot," *IEEE Transactions on Systems, Man and Cybernetics, Part A: Systems and Humans*, vol. 29, no. 3, pp. 255–268, May 1999.

[30] H. Park, K. Sreenath, A. Ramezani, and J. W. Grizzle, "Switching control design for accommodating large step-down disturbances in bipedal robot walking," in *IEEE International Conference on Robotics and Automation*, May 2012, to appear.

[31] J. Pratt and G. Pratt, "Intuitive control of a planar bipedal walking robot," in *Proc. IEEE International Conference on Robotics and Automation*, vol. 3, pp. 2014–2021, 16-20 May 1998.

[32] H. Park, K. Sreenath, J. Hurst, and J. W. Grizzle, "Identification of a Bipedal Robot with a Compliant Drivetrain: Parameter estimation for control design," *IEEE Control Systems Magazine*, vol. 31, no. 2, pp. 63–88, Apr. 2011.

[33] S. S. Ha, J. H. Yu, Y. J. Han, and H. S. Hahn, "Natural Gait Generation of Biped Robot based on Analysis of Human's Gait," in *International Conference on Smart Manufacturing Application*, pp. 30–34, Apr. 2008.

[34] T. Yang, E. Westervelt, A. Serrani, and J. Schmiedeler, "A framework for the control of stable aperiodic walking in underactuated planar bipeds," *Autonomous Robots*, vol. 27, no. 3, pp. 277–290, 2009.

[35] A. D. Ames, "First Steps Toward Automatically Generating Bipedal Robotic Walking from Human Data," in *8th International Workshop on Robotic Motion and Control*, Poland, 2011.

[36] A. D. Ames, "First Steps Toward Underactuated Human-Inspired Bipedal Robotic Walking," in *IEEE International Conference on Robotics and Automation*, May 2012, to appear.

[37] L. Yang, C. Chew, T. Zielinska, and A. Poo, "A uniform biped gait generator with offline optimization and online adjustable parameters," *Robotica*, vol. 25, no. 5, pp. 549–565, 2007.

[38] Y. Xiang, J. S. Arora, H. J. Chung, H. J. Kwon, S. Rahmatalla, R. Bhatt, and K. Abdel-Malek., "Predictive simulation of human walking transitions using an optimization formulation," *Structural and Multidisciplinary Optimization*, vol. 45, no. 5, pp. 759–772, 2012.

[39] S. Nadubettu Yadukumar, M. Pasupuleti and A. D. Ames, "From Formal Methods to Algorithmic Implementation of Human Inspired Control on Bipedal Robots," in *Proc. of 10th International Workshop on the Algorithmic Foundations of Robotics (WAFR)*, 2012, to appear.

[40] T. Burg, D. Dawson, J. Hu, and M. de Queiroz, "An adaptive partial state-feedback controller for RLED robot manipulators," *IEEE Transactions on Automatic Control*, vol. 41, no. 7, pp. 1024–1030, Jul. 1996.

[41] C. Liu, C. C. Cheah and J. E. Slotine, "Adaptive Jacobian tracking control of rigid-link electrically driven robots based on visual task-space information," *Automatica*, vol. 42, no. 9, pp. 1491–1501, 2006.

[42] *Robustness tests on the Bipedal Robot AMBER.* (2012, May 14) [Online]. Available at: http://www.youtube.com/watch?v=RgQ8atV1NW0

[43] J. W. Grizzle, C. Chevallereau, A. D. Ames, and R. W. Sinnet, "3D Bipedal Robotic Walking: Models, Feedback Control, and Open Problems," in *8th IFAC Symposium on Nonlinear Control Systems*, Bologna, Italy, Sep. 2010.

[44] M. Pasupuleti, S. Nadubettu Yadukumar and A. D. Ames, "Human Inspired Underactuated Bipedal Robotic Walking with AMBER on Flatground, Upslope and Uneven Terrain," submitted to *IEEE/ RSJ International Conference on Intelligent Robots and Systems (IROS)*, 2012.

[45] E. Wendel and A. D. Ames, "Rank Properties of Poincaré maps for hybrid systems with applications to bipedal walking," in *Proc. of Hybrid Systems: Computation and Control*, Stockholm, Sweden, 2010.

[46] B. Morris and J. W. Grizzle, "A Restricted Poincaré Map for Determining Exponentially Stable Periodic Orbits in Systems with Impulse Effects: Application to Bipedal Robots," in *IEEE Conference on Decision and Control*, Seville, Spain, Dec. 2005.

[47] S. S. Sastry, *Nonlinear Systems: Analysis, Stability and Control.* New York: Springer, Jun. 1999.

[48] M. W. Spong and F. Bullo, "Controlled Symmetries and Passive Walking," *IEEE Transactions on Automatic Control*, vol. 50, no. 7, pp. 1025–1031, 2005.

[49] R. Vasudevan, A. D. Ames and R. Bajcsy, "Using Persistent Homology to Determine a Human-Data Based Cost for Bipedal Walking," in *18th IFAC World Congress*, Milano, Italy, 2011.

[50] J. W. Grizzle, J. Hurst, B. Morris, H. Park, and K. Sreenath, "MABEL, A New Robotic Bipedal Walker and Runner," in *American Control Conference*, pp. 2030–2036, St. Louis, USA, Jun. 2009.

[51] *System Identification Toolbox.* (2012, May 14) [Online]. Available at: http://www.mathworks.com/help/toolbox/ident/gs/bqyzc00.html

[52] *Human-Inspired Proportional Control with AMBER in simulation.* (2012, May 14) [Online]. Available at: http://www.youtube.com/watch?v=z3oPzlStzRo

[53] *AMBER walking with Human-Inspired Control*. (2012, May 14) [Online]. Available at: http://www.youtube.com/watch?v=SYXWoNU8QUE

[54] *Virtex-5 FPGA Family Overview*. (2012, May 14) [Online]. Available at: http://www.xilinx.com/support/documentation/data_sheets/ds100.pdf

[55] *NAO V3.3 H25 model motors*. (2012, May 14) [Online]. Available at: http://www.aldebaran-robotics.com/documentation/nao/hardware/kinematics/motors.html

[56] *DARwIn-OP with Dynamixel RX28 motors*. (2012, May 14) [Online]. Available at: http://darwin-op.springnote.com

[57] *Maxon Motor REmax-24 Brushed DC Motor*. (2012, May 14) [Online]. Available at: http://www.maxonmotor.com/medias/sys_master/8796801728542/RE-max-24-222048_11_EN_130.pdf

APPENDIX A

ADDITIONAL FIGURES

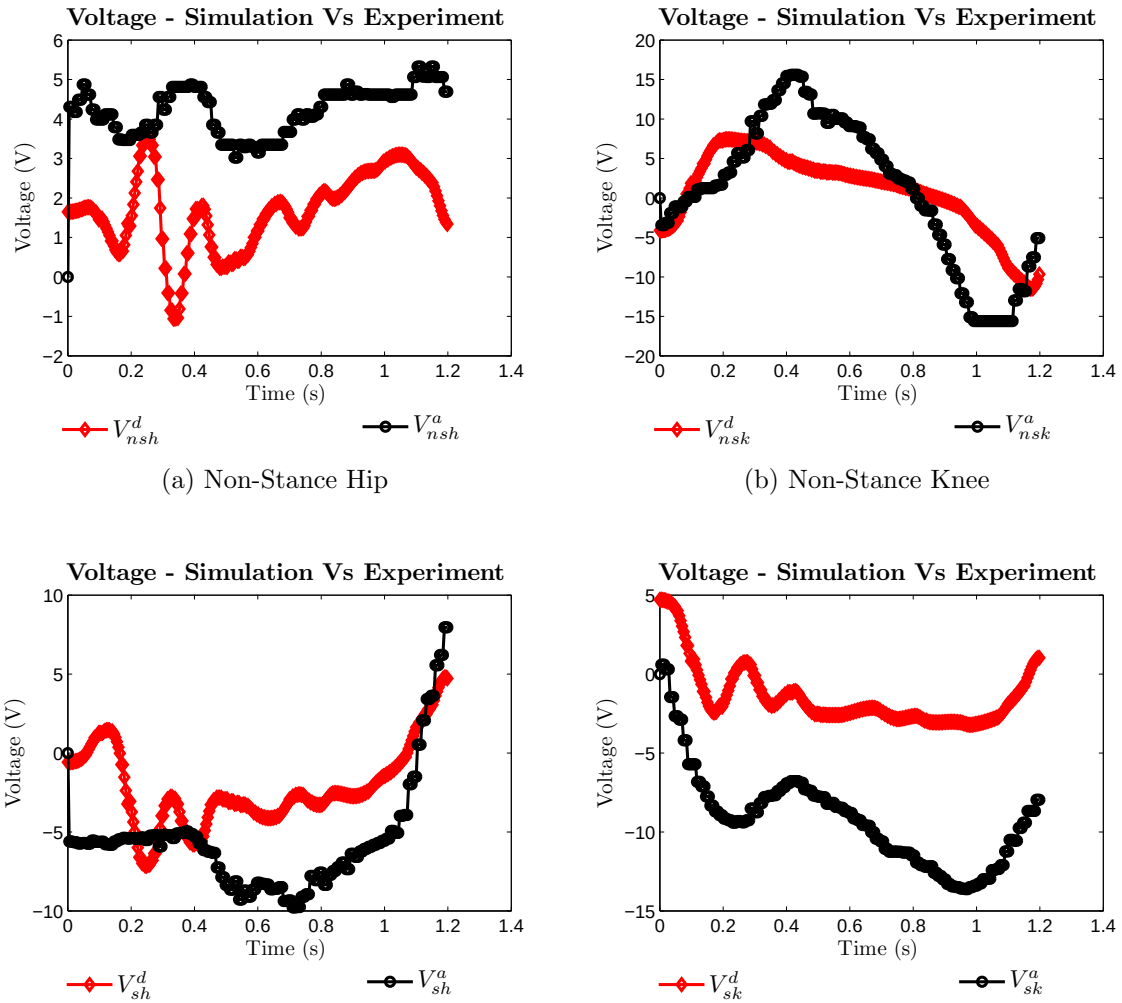

(a) Non-Stance Hip

(b) Non-Stance Knee

(c) Stance Hip

(d) Stance Knee

Fig. A.1.: Voltage-based P-control experiment vs simulation for one step: black lines indicate the actual voltage applied to a DC motor based on AMBER configuration during experimental walking, while the red lines indicate the voltage input generated in simulation using a reduced DC motor model with inductance ignored.

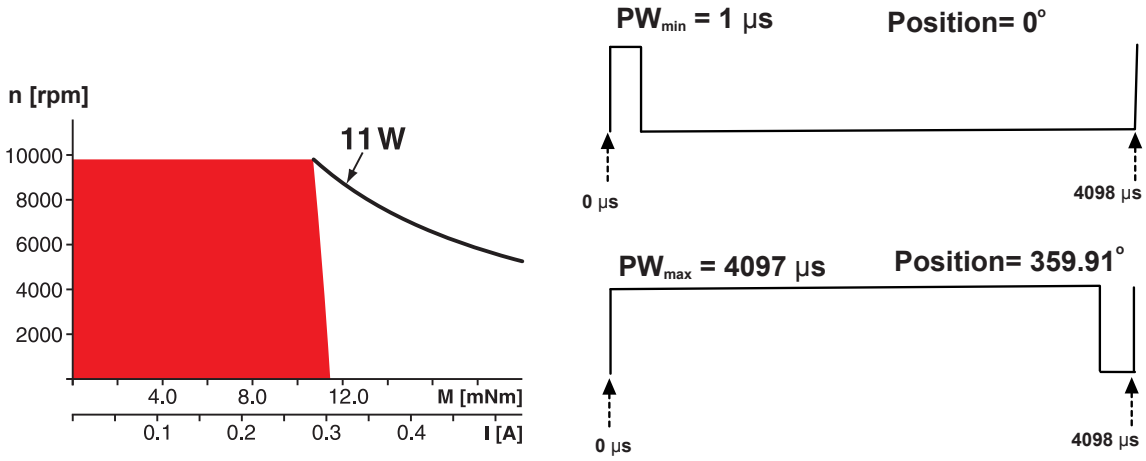

Fig. A.2.: (a.) DC motor operation: speed vs torque characteristics ([57]). (b.) PWM pulse recieved from the absolute encoder which is used to calculate the joint angles.

APPENDIX B

LABVIEW FPGA SUBMODULES

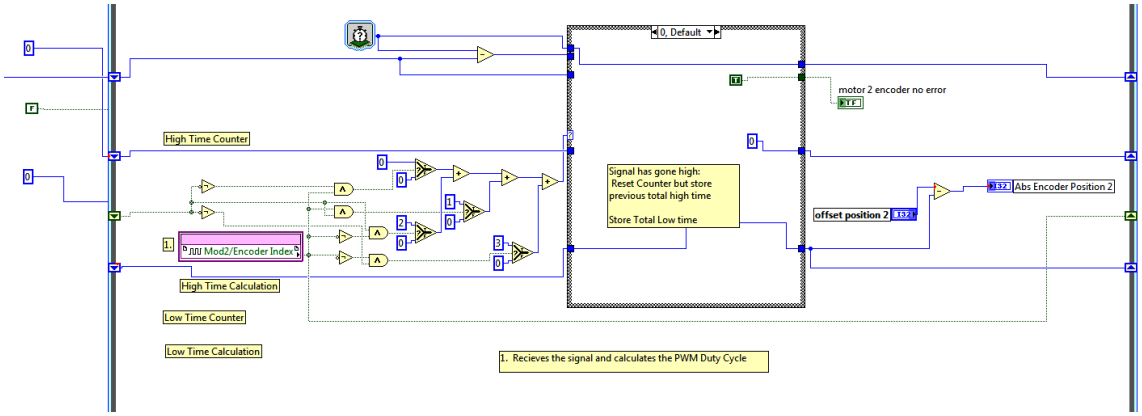

(a)

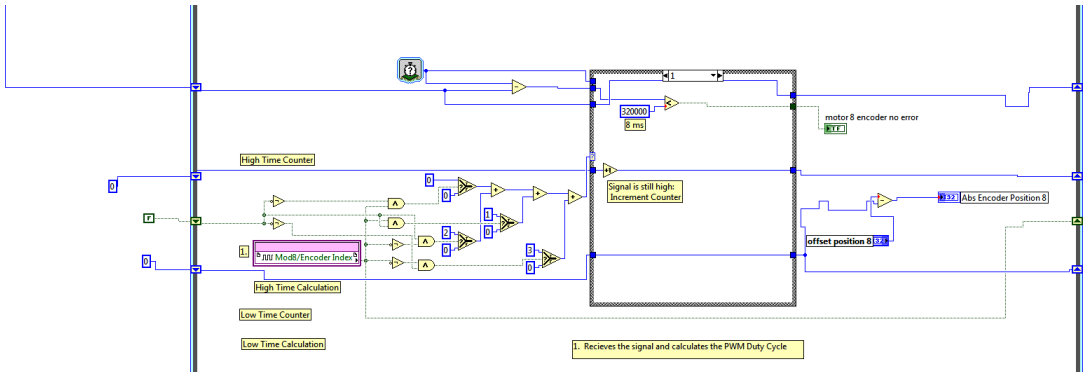

(b)

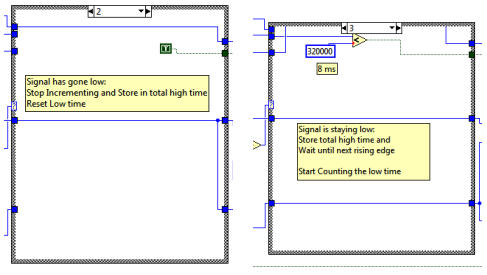

(c) (d)

Fig. B.1.: LabVIEW FPGA schematic used for angle calculation and error flag generation from absolute encoder pulse.

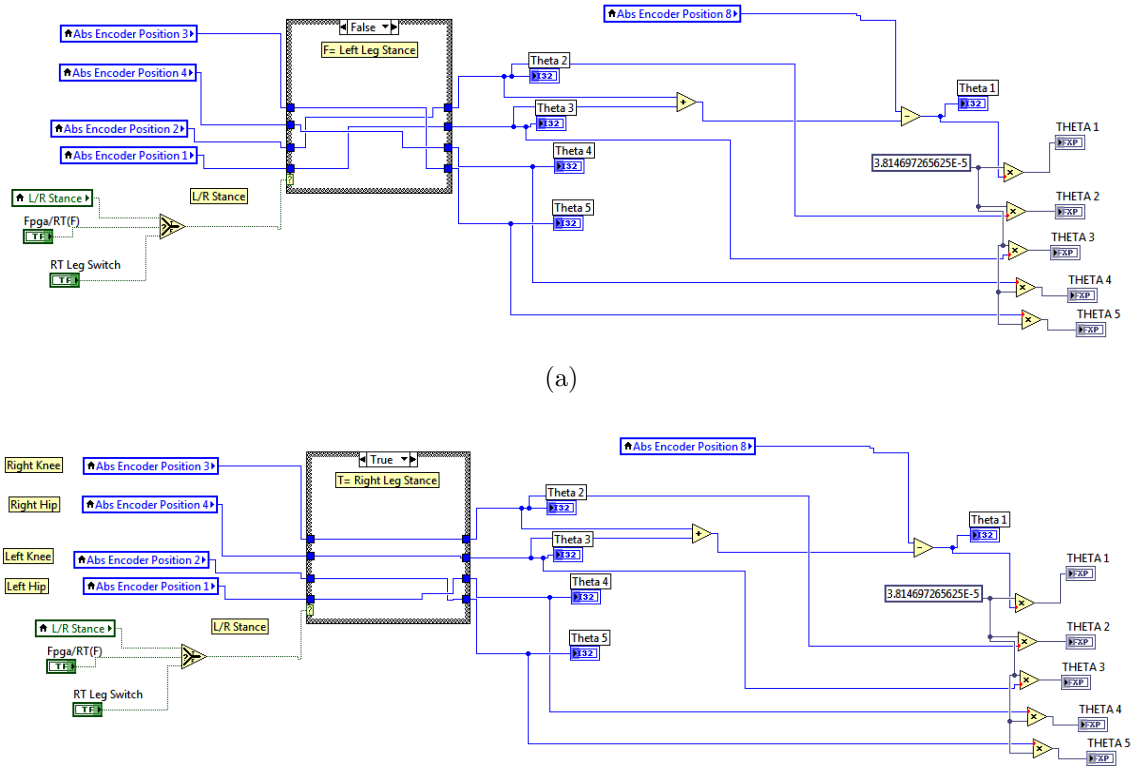

Fig. B.2.: LabVIEW FPGA schematic used for discrete dynamics operation — angles (leg) switching after guard detection.

VITA

Murali Krishna Pasupuleti is from Kakinada, India. He completed his Bachelor of Technology in electrical and electronics engineering from the National Institute of Technology, Warangal, India in May 2008. He went on to pursue his graduate studies in electrical engineering at Texas A&M University and graduated with his M.S. in August 2012. His research interests are in robotics, nonlinear control, and digital hardware controller implementations. His mailing address is: 422 James J. Cain 51 Bldg, 3123 TAMU, College Station, TX 77843, and he can be reached on email at: murali.ilarum@gmail.com.